SANDIA REPORT

SAND2015-20731
Unlimited Release
January 2015

Parameterized Receptacle-Pin Contact Model

Matthew David Williams

Prepared by
Sandia National Laboratories
Albuquerque, New Mexico 87185 and Livermore, California 94550

Sandia National Laboratories is a multi-program laboratory managed and operated by Sandia Corporation, a wholly owned subsidiary of Lockheed Martin Corporation, for the U.S. Department of Energy's National Nuclear Security Administration under contract DE-AC04-94AL85000.

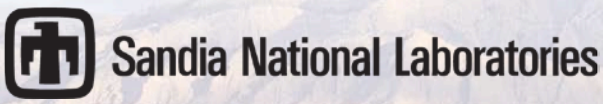

Issued by Sandia National Laboratories, operated for the United States Department of Energy by Sandia Corporation.

Available to DOE and DOE contractors from
U.S. Department of Energy
Office of Scientific and Technical Information
P.O. Box 62
Oak Ridge, TN 37831

Telephone: (865) 576-8401
Facsimile: (865) 576-5728
E-Mail: reports@adonis.osti.gov
Online ordering: http://www.osti.gov/bridge

Available to the public from
U.S. Department of Commerce
National Technical Information Service
5285 Port Royal Rd.
Springfield, VA 22161

Telephone: (800) 553-6847
Facsimile: (703) 605-6900
E-Mail: orders@ntis.fedworld.gov
Online order: http://www.ntis.gov/help/ordermethods.asp?loc=7-4-0#online

SAND2015-20731
Unlimited Release
January 2015

Parameterized Receptacle-Pin Contact Model

Matthew David Williams
Electromechanical Systems II, 02615
Sandia National Laboratories
P.O. Box 5800
Albuquerque, New Mexico 87185-MS0333

Abstract

This report describes a simple, quasi-static, closed-form, parameterized model that predicts the contact forces acting between axially-engaging electrical contact receptacles and a pin. This approach is useful for design studies and reduced-order mechanism modeling, where receptacle-pin insertion forces have traditionally been difficult to quantify without high-fidelity (e.g. rigid body dynamics, finite element analysis) simulations. A Matlab implementation of the model is provided and is demonstrated for three receptacle geometries. Results are compared to rigid body dynamics simulations for the first two geometries and experimental insertion force measurements for the third.

ACKNOWLEDGMENTS

The genesis of this modeling effort came from Coby Davis (then of 02616, now of 02624), whose desire for physics-based assessments of mechanism performance aging led the author to seek a fast, simple approach for estimating contact forces in mechanisms. Luke Zsiga (02615) has also been supportive of that ideal. The generous ongoing support of component leads Gil Benavides (02616), Cathy Siefert (02615), and Ray Ely (02614) toward mechanism modeling, model calibration, and parameter extraction work has been critical to the creation of this document. The author would also like to thank Jordan Massad, Matt Brake, and Lin Zheng (01526) for embracing the contact model in their reduced-order modeling and robust optimization efforts. They were the ones who truly demonstrated the model's value and ultimately encouraged the creation of this document and the expansion of the model's capabilities from its original state. Thanks are also due to Mike Sena (02615) for providing experimental measurements of insertion force between a bifurcated receptacle and a pin and Johann Snyder (02616) for his assistance with finalizing this document.

CONTENTS

FIGURES

TABLES

NOMENCLATURE

DOE	Department of Energy
LMS VLM	LMS Virtual.Lab Motion
RBD	Rigid body dynamics
SNL	Sandia National Laboratories

Page Intentionally Left Blank

1. INTRODUCTION

The operation of many mechanisms within the Sandia National Laboratories portfolio involves the closure of electrical circuits. A common geometry used for electrical circuit closure is that of a bifurcated receptacle expanding over a pin as in Figure 1. In the past, the forces associated with the receptacle-to-pin interface have been challenging to predict over the entirety of the stroke without direct use of the solid model geometry and contact algorithms in a full-fidelity rigid body dynamics (RBD) model or finite element model. In lieu of this full-fidelity approach, this report describes a simple method for predicting the contact forces in closed-form, enabling the inclusion of greater fidelity in efficient, reduced-order modeling approaches. Approaches such as ODE-based formulations of mechanisms in Matlab are valuable for early design studies or statistical performance characterization (e.g. Monte Carlo analysis and robust optimization).

The receptacle-pin contact model is documented in this report with extensive detail. The primary underlying assumption in the creation of this model is that the receptacle and pin remain in continuous contact. This assumption implies that pin insertion must be effectively quasi-static such that the receptacle arms do not "bounce" or otherwise lose contact with the pin. The model is fully parameterized to allow studies of sensitivity of forces to receptacle/pin geometry (including imperfection in the receptacle arms) and receptacle stiffness. The entire mathematical approach is discussed in detail in Section 2. The model is validated for test cases against RBD simulations and experimental measurements in Section 3. A functionalized version of the model for use in Matlab and example input decks are provided in Appendix B.

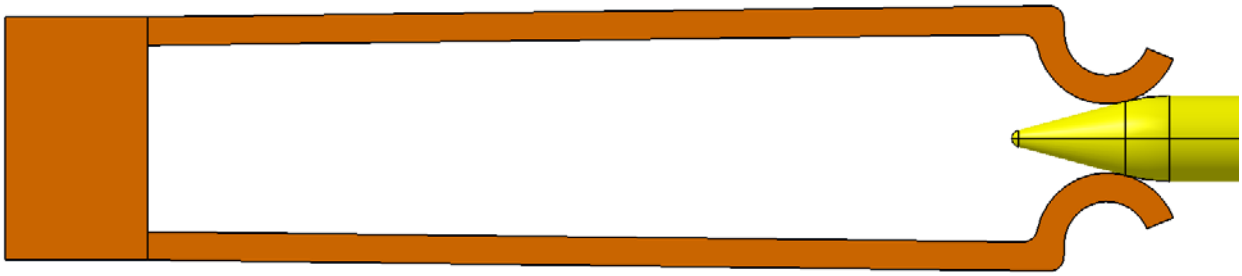

Figure 1. Bifurcated receptacle engaging a pin.

2. CONTACT MODELING

This section describes the receptacle-pin contact model in considerable detail. The ultimate goal of the contact model is to enable determination of the contact forces acting on a receptacle (or pin) as insertion progresses. In Section 2.1, the relationship between the contact forces, the receptacle stiffness, and receptacle deflection is established. In Section 2.2, kinematic equations are derived based on a geometric parameterization of the receptacle and pin geometries. Section 2.3 addresses some issues of compatibility in the geometric parameterization, Section 2.4 makes some distinctions between modeling of an engaging receptacle vs. a disengaging receptacle, and Section 2.5 discusses important numerical considerations when using the model as part of a larger dynamic simulation.

2.1. Forces

This section discusses the relationship between the receptacle deflection and contact force. A receptacle arm is essentially a cantilever beam whose deflection may be approximated via a pseudo-rigid body model (Howell, 2001) as

$$K\theta = M\,, \tag{1.1}$$

where M is the applied moment, θ is the rigid body rotation of the beam, and K is its stiffness. This approach effectively places a torsional spring at the cantilever end of the beam that resists deflection due to an applied force (or equivalent moment). Figure 2 shows a notional geometry with this approximation applied to the receptacle arm. For quasi-static motion, the normal and tangential components F_n and F_t, respectively, contribute to the applied moment M as

$$K\theta = F_n L_{mn} - F_t L_{mt}\,, \tag{1.2}$$

where the moment arms L_{mn} and L_{mt} are the perpendicular distances from point O to the line of action of F_n and F_t, respectively. For a particular receptacle and pin geometry, the values of θ, L_{mn}, and L_{mt} may be determined from knowledge of the contact point and orientation of the contact surfaces. Finding these variables from kinematic considerations is the purpose of Section 2.2; for now, the goal is to determine expressions for the normal and tangential forces with the other variables taken as known. First, a constitutive law (Coulomb friction) is used to relate the normal and tangential forces as

$$F_t = \mu F_n\,, \tag{1.3}$$

where μ is the friction coefficient. Substituting (1.3) into (1.2) and rearranging yields an equation for the normal force,

$$F_n = \frac{K\theta}{L_{mn} - \mu L_{mt}}\,. \tag{1.4}$$

Equation (1.4) can be solved for the normal force and then the tangential force is easily found from (1.3). The normal and tangential forces can then be decomposed into the x and y coordinate directions (reference Figure 2) as

$$F_x = -F_n \sin\alpha - F_t \cos\alpha \tag{1.5}$$

and

$$F_y = F_n \cos\alpha - F_t \sin\alpha\,, \tag{1.6}$$

where α is the angle of the outward pin surface normal relative to the y-axis (positive sense determined by right hand rule, see Figure 2). The force F_x is often the primary quantity of interest and is known as the *insertion force*.

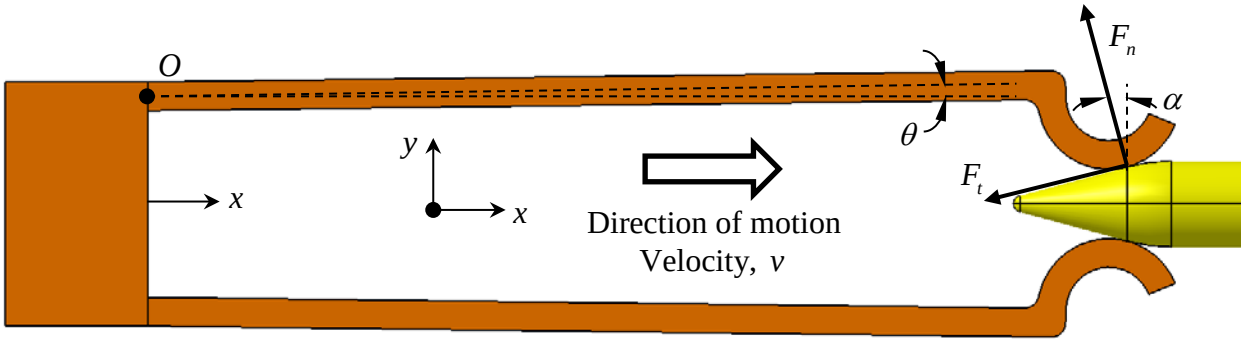

Figure 2. Simple example of receptacle-pin insertion.

2.2. Kinematic Equations

In this section, the kinematic equations for the receptacle deflection θ, the angle of the normal force α, and the moment arms L_{mn} and L_{mt} are derived. The equations are derived via vector loops. Typically, one loop is used to determine θ (and α if necessary) while a second loop is used to determine L_{mn} and L_{mt}. Equations are found in a piece-wise sense; that is, separate sets of equations are used for receptacle contact with the pin tip, cone, round, and barrel, respectively. Configurations of the receptacle and pin that occur at the transitions between equation sets (e.g. in the transition from pin cone to round or round to barrel) are called "critical values" and are determined as well.

To add additional utility to the model, the kinematic equations throughout the following sub-sections include initial angular imperfection in the receptacle arm, θ_0 (not shown in Figure 2). The total angular deflection from horizontal (x-direction in Figure 2) is thus

$$\theta^* = \theta + \theta_0\,, \tag{1.7}$$

where θ_0 is the initial (unstressed) angular deflection from horizontal and θ is the incremental angular deflection due to applied forces. Because θ_0 describes an unstressed configuration, only

the incremental deflection θ appears in the normal force expression, (1.4). For the pseudo-rigid body model to remain valid, it is a good rule of thumb that θ must be sufficiently small to satisfy the small angle approximation.

2.2.1. Receptacle on Pin Tip

Figure 3 shows a simplified geometric diagram for a receptacle arm in contact with a pin tip (image is not to typical scale in order to show the different geometric features with clarity). In this diagram, most dimensions are fixed geometric parameters, though some dimensions are variables associated with the motion of the receptacle arm (e.g. d, θ, L_{mn}, and L_{mt}).

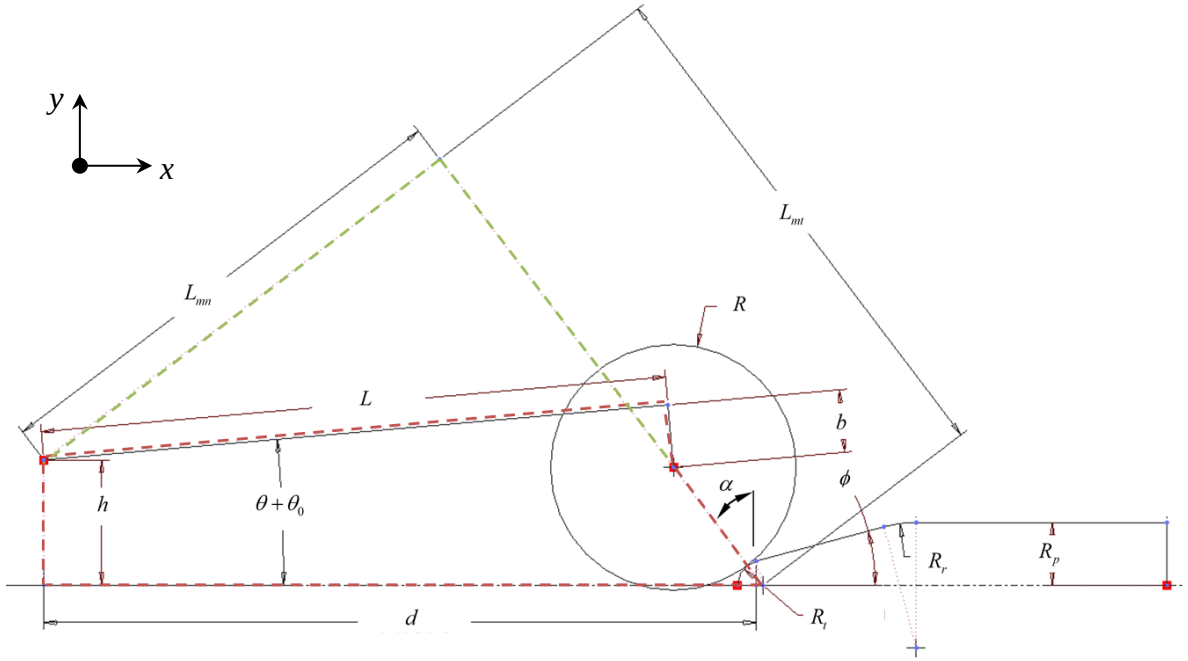

Figure 3. Geometric diagram for receptacle on pin tip.

As the receptacle arm engages the pin (moves to the right), the separation distance, d, decreases. Letting the initial separation distance be denoted as d_0, the separation distance as a function of receptacle displacement x from this initial configuration is

$$d = d_0 - x\,. \tag{1.8}$$

Referring to Figure 3, the vector loop equations are

$$d + R_t - (R_t + R)\sin\alpha - b\sin\theta^* - L\cos\theta^* = 0 \tag{1.9}$$

and

$$-h + (R_t + R)\cos\alpha + b\cos\theta^* - L\sin\theta^* = 0\,. \tag{1.10}$$

Here, d (or rather x via (1.8)) is the control parameter and both θ^* and α are dependent on position. Moving the terms containing α to the right hand sides, squaring both equations (1.9) and (1.10), and then summing them gives

$$\left(d + R_t - b\sin\theta^* - L\cos\theta^*\right)^2 + \left(h - b\cos\theta^* + L\sin\theta^*\right)^2 = \left(R_t + R\right)^2, \tag{1.11}$$

which after expansion and rearrangement yields

$$L^2 + b^2 + h^2 + \left(R_t + d\right)^2 - \left(R_t + R\right)^2 - 2\left[L\left(R_t + d\right) + bh\right]\cos\theta^* + 2\left[Lh - b\left(R_t + d\right)\right]\sin\theta^* = 0 \tag{1.12}$$

which is in the form

$$A + B\cos\theta^* + C\sin\theta^* = 0 \tag{1.13}$$

with

$$A = L^2 + b^2 + h^2 + \left(R_t + d\right)^2 - \left(R_t + R\right)^2 , \tag{1.14}$$

$$B = -2\left[L\left(R_t + d\right) + bh\right] , \tag{1.15}$$

and

$$C = 2\left[Lh - b\left(R_t + d\right)\right] . \tag{1.16}$$

The solution of (1.13) for θ^* via trigonometric manipulations and the quadratic equation is discussed in Appendix A-- see Equation (1.89) and (1.91). With θ^* known from the solution of (1.12)/(1.13), the normal force angle α can then be found from (1.10) as

$$\alpha = \cos^{-1}\frac{L\sin\theta^* - b\cos\theta^* + h}{R_t + R}, \tag{1.17}$$

where $\alpha = 90^\circ$ for contact with the pin tip and $\alpha = \phi$ for contact at the tip-to-cone transition.

The moment arms are found from the vector loop equations

$$d + R_t - \left(R_t + L_{mt}\right)\sin\alpha - L_{mn}\cos\alpha = 0 \tag{1.18}$$

and

$$-h + \left(R_t + L_{mt}\right)\cos\alpha - L_{mn}\sin\alpha = 0 , \tag{1.19}$$

which when solved simultaneously give

$$L_{mn} = \left(R_t + d\right)\cos\alpha - h\sin\alpha \tag{1.20}$$

and

$$L_{mt} = \left(R_t + d\right)\sin\alpha + h\cos\alpha - R_t . \tag{1.21}$$

At the first critical value of d and θ^*, the receptacle contacts the very tip of the pin ($\alpha = 90^\circ$), which from (1.10) reveals

$$-h + b\cos\theta^*_{cr,1} - L\sin\theta^*_{cr,1} = 0\ , \tag{1.22}$$

which is in the standard form with $A = -h$, $B = b$, and $C = -L$. With $\theta^*_{cr,1}$ known, $d_{cr,1}$ is found from (1.9) to be

$$d_{cr,1} = b\sin\theta^*_{cr,1} + L\cos\theta^*_{cr,1} + R\,. \tag{1.23}$$

The transition from the pin tip to cone is the second critical transition. Letting $\alpha = \phi$ in (1.10) gives

$$-h + \left(R_t + R\right)\cos\phi + b\cos\theta^*_{cr,2} - L\sin\theta^*_{cr,2} = 0 \tag{1.24}$$

which is in the standard form with $A = -h + \left(R_t + R\right)\cos\phi$, $B = b$, and $C = -L$. With $\theta^*_{cr,2}$ known from (1.24), $d_{cr,2}$ is found from (1.9) to be

$$d_{cr,2} = b\sin\theta^*_{cr,2} + L\cos\theta^*_{cr,2} + \left(R_t + R\right)\sin\phi - R_t\,. \tag{1.25}$$

The equations in this section are valid for receptacle contact with the pin tip that causes the receptacle to deflect in the correct (whether positive or negative) sense. For this to occur, it must be true that θ takes the correct non-zero sign over some part of the range $d_{cr,1} \le d \le d_{cr,2}$. For example, in the geometry as drawn in Figure 3, $\theta > 0$ indicates the pin causes the receptacle to deflect outward, while $\theta < 0$ indicates the receptacle would have to bend inward to touch the pin. Therefore, in this case, the final value of θ utilized (call it θ_f) is the maximum of the value of θ found from the equations of this section or zero. To expand the robustness of the model to cases that don't quite so closely resemble Figure 3, the selection criteria

$$\theta_f = \max\left\{\mathrm{sgn}\left[\cos\left(\theta_0\right)\right]\theta, 0\right\}\mathrm{sgn}\left[\cos\left(\theta_0\right)\right] \tag{1.26}$$

is recommended, where in this case θ is the solution to (1.12) for $d_{cr,2} \le d \le d_{cr,1}$. This effectively selects positive θ for $\cos\theta_0 > 0$ (zero otherwise) and negative θ for $\cos\theta_0 < 0$ (zero otherwise) while retaining the sign, which accommodates problems, for example, where $\theta_0 = \pm 180°$ (see Section 3.1.2). This expression breaks down at $\theta_0 = \pm 90°$ (zero is always selected).

If contact first occurs on the pin tip, i.e. over the range $d_{cr,2} \le d \le d_{cr,1}$, then the receptacle-pin separation distance at contact, d_c , is

$$d_c = -R_t + \left(R_t + R\right)\sin\alpha_c + b\sin\theta_0 + L\cos\theta_0 \tag{1.27}$$

with

$$\alpha_c = \cos^{-1}\frac{L\sin\theta_0 - b\cos\theta_0 + h}{R_t + R}. \tag{1.28}$$

2.2.2. Receptacle on Pin Cone

Figure 4 shows the receptacle in contact with the pin cone. As x increases (the separation distance d decreases), the contact point travels along the pin cone a distance L_c.

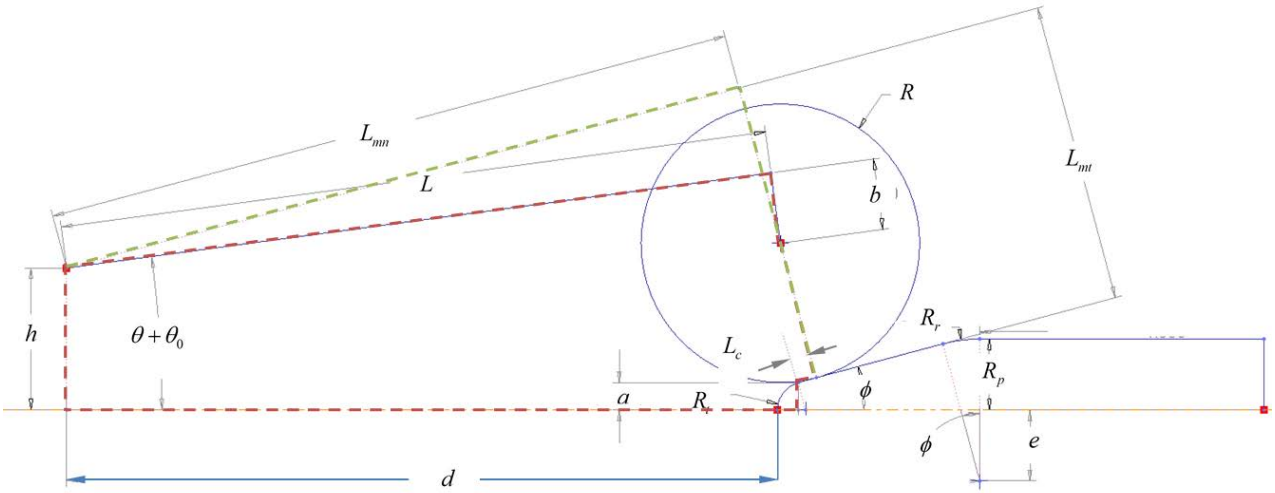

Figure 4. Geometric diagram for receptacle on pin cone.

Referring to Figure 4, the vector loop equations for finding θ^* are

$$d + R_t - R_t\sin\phi + L_c\cos\phi - R\sin\phi - b\sin\theta^* - L\cos\theta^* = 0 \tag{1.29}$$

and

$$-h + a + L_c\sin\phi + R\cos\phi + b\cos\theta^* - L\sin\theta^* = 0, \tag{1.30}$$

which are written for the x and y coordinate directions, respectively. Solving the second equation for L_c gives

$$L_c = \frac{h - a - R\cos\phi - b\cos\theta^* + L\sin\theta^*}{\sin\phi}. \tag{1.31}$$

Substituting (1.31) into (1.29) and regrouping into common terms of θ^* gives

$$\left[d + R_t - (R_t + R)\sin\phi + \frac{h - a - R\cos\phi}{\tan\phi}\right] - \left(L + \frac{b}{\tan\phi}\right)\cos\theta^* + \left(\frac{L}{\tan\phi} - b\right)\sin\theta^* = 0, \tag{1.32}$$

with coefficients of

$$A = d + R_t - (R_t + R)\sin\phi + \frac{h - a - R\cos\phi}{\tan\phi}, \tag{1.33}$$

$$B = -\left(L + \frac{b}{\tan\phi} \right), \tag{1.34}$$

and

$$C = \frac{L}{\tan\phi} - b\,. \tag{1.35}$$

The moment arms L_{mn} and L_{mt} are found from the simultaneous solution of the second vector loop, with equations

$$d + R_t - R_t \sin\phi + L_c \cos\phi - L_{mt} \sin\phi - L_{mn} \cos\phi = 0 \tag{1.36}$$

and

$$-h + a + L_c \sin\phi + L_{mt} \cos\phi - L_{mn} \sin\phi = 0 \tag{1.37}$$

written for the x and y coordinate directions, respectively. The solutions are

$$\begin{aligned} L_{mn} &= \left(d + R_t - R_t \sin\phi\right)\cos\phi - (h-a)\sin\phi + L_c \\ &= \left(d + R_t - R_t \sin\phi\right)\cos\phi - (h-a)\sin\phi + \frac{h - a - R\cos\phi - b\cos\theta^* + L\sin\theta^*}{\sin\phi} \end{aligned} \tag{1.38}$$

and

$$L_{mt} = \left(d + R_t\right)\sin\phi + R_t \cos^2\phi - R_t + \left(h - a\right)\cos\phi\,. \tag{1.39}$$

The angle associated with the normal force is constant as long as contact is maintained with the pin cone. It is simply

$$\alpha = \phi\,. \tag{1.40}$$

In summary, (1.32) for θ^* and (1.38)-(1.39) for L_{mn} and L_{mt} are valid for $d_{cr,3} \le d \le d_{cr,2}$, where $d_{cr,2}$ was given in (1.25) and $d_{cr,3}$ is discussed in the next section. If contact first occurs over this range of validity, then the receptacle-pin separation distance at contact, d_c, is

$$d_c = -R_t + R_t \sin\phi - L_c\left(\theta_0\right)\cos\phi + R\sin\phi + b\sin\theta_0 + L\cos\theta_0 \tag{1.41}$$

where from (1.31),

$$L_c\left(\theta_0\right) = \frac{h - a - R\cos\phi - b\cos\theta_0 + L\sin\theta_0}{\sin\phi}\,. \tag{1.42}$$

2.2.3. Receptacle on Pin Round

Figure 5 shows a geometric diagram for a receptacle arm in contact with a pin cone-to-barrel round. While the pin round is traversed, the normal angle α transitions from ϕ to 0 from the pin cone to the pin barrel.

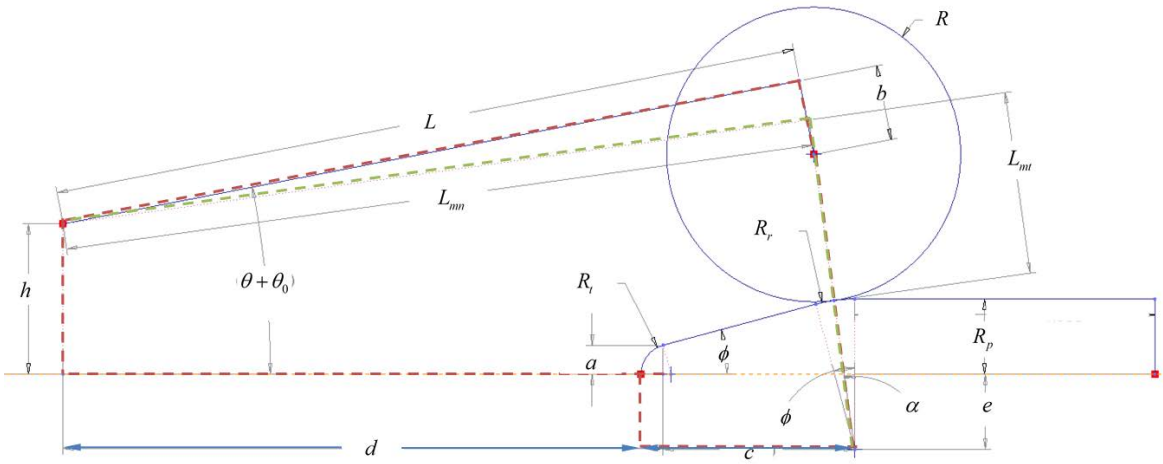

Figure 5. Geometric diagram for receptacle on pin round.

Referring to Figure 5, the first set of vector loop equations are

$$d + c - \left(R + R_r\right)\sin\alpha - b\sin\theta^* - L\cos\theta^* = 0 \tag{1.43}$$

and

$$-h - e + \left(R + R_r\right)\cos\alpha + b\cos\theta^* - L\sin\theta^* = 0\,. \tag{1.44}$$

Rearranging both equations, squaring both sides, and then adding yields

$$\left(R + R_r\right)^2 = \left(d + c - b\sin\theta^* - L\cos\theta^*\right)^2 + \left(L\sin\theta^* - b\cos\theta^* + h + e\right)^2 \tag{1.45}$$

Expanding the right hand side gives

$$\left(R + R_r\right)^2 = L^2 + b^2 + \left(d + c\right)^2 + \left(h + e\right)^2 - 2\left(d + c\right)\left(b\sin\theta^* + L\cos\theta^*\right) + 2\left(h + e\right)\left(L\sin\theta^* - b\cos\theta^*\right) \tag{1.46}$$

which can be rearranged into the standard form of (1.86),

$$\left(R + R_r\right)^2 - L^2 - b^2 - \left(d + c\right)^2 - \left(h + e\right)^2 + 2\left[L\left(d + c\right) + b\left(h + e\right)\right]\cos\theta^* + 2\left[b\left(d + c\right) - L\left(h + e\right)\right]\sin\theta^* = 0 \tag{1.47}$$

Equation (1.47) may be solved via (1.91) with coefficients

$$A = \left(R + R_r\right)^2 - L^2 - b^2 - \left(d + c\right)^2 - \left(h + e\right)^2, \tag{1.48}$$

$$B = 2L\left(d + c\right) + 2b\left(h + e\right), \tag{1.49}$$

and

$$C = 2b\left(d + c\right) - 2L\left(h + e\right). \tag{1.50}$$

The angle of the pin round normal at the contact point may be found from (1.44) as

$$\alpha = \cos^{-1}\frac{L\sin\theta^* - b\cos\theta^* + h + e}{R + R_r}. \tag{1.51}$$

The moment arms are found from simultaneous solution of the vector loop equations

$$d + c - \left(R_r + L_{mt}\right)\sin\alpha - L_{mn}\cos\alpha = 0 \tag{1.52}$$

$$-h - e + \left(R_r + L_{mt}\right)\cos\alpha - L_{mn}\sin\alpha = 0, \tag{1.53}$$

which when solved simultaneously yield the simple expressions

$$L_{mn} = \left(d + c\right)\cos\alpha - \left(h + e\right)\sin\alpha \tag{1.54}$$

and

$$L_{mt} = \left(d + c\right)\sin\alpha + \left(h + e\right)\cos\alpha - R_r. \tag{1.55}$$

Note that in any of these equations, a consistent set of the variables d, θ, and α must be used that satisfy (1.47) and (1.51).

Validity of equations (1.43)-(1.55) is bounded by $\phi \geq \alpha \geq 0$ (points at which the pin cone meets the pin round and the pin round meets the pin barrel). The condition $\alpha = \phi$ corresponds to the critical points $\theta^*_{cr,3}$ and $d_{cr,3}$ while the condition $\alpha = 0$ corresponds to the critical points $\theta^*_{cr,4}$ and $d_{cr,4}$. Utilizing the former condition with (1.43) and (1.44) gives

$$d_{cr,3} + c - \left(R + R_r\right)\sin\phi - b\sin\theta^*_{cr,3} - L\cos\theta^*_{cr,3} = 0 \tag{1.56}$$

and

$$-\left(h + e\right) + \left(R + R_r\right)\cos\phi + b\cos\theta^*_{cr,3} - L\sin\theta^*_{cr,3} = 0. \tag{1.57}$$

Equation (1.57) is in the standard form for finding $\theta^*_{cr,3}$ (or $\theta_{cr,3} = \theta^*_{cr,3} - \theta_0$) via Equation (1.91) with coefficients

$$A = \left(R + R_r\right)\cos\phi - \left(h + e\right), \tag{1.58}$$

$$B = b, \tag{1.59}$$

and

$$C = -L. \tag{1.60}$$

With $\theta^*_{cr,3}$ known, (1.56) then gives the critical value of $d_{cr,3}$ as

$$d_{cr,3} = -c + \left(R + R_r\right)\sin\phi + b\sin\theta^*_{cr,3} + L\cos\theta^*_{cr,3}. \tag{1.61}$$

The second set of critical points at $\alpha = 0$ is found similarly from equations (1.43) and (1.44), giving

$$d_{cr,4} + c - b\sin\theta^*_{cr,4} - L\cos\theta^*_{cr,4} = 0 \tag{1.62}$$

$$R + R_p - h + b\cos\theta^*_{cr,4} - L\sin\theta^*_{cr,4} = 0 \tag{1.63}$$

where the substitution $R_p = R_r - e$ was made. Equation (1.63) is in the standard form and can be solved for $\theta^*_{cr,4}$ via Equation (1.91) and the coefficients

$$A = R + R_p - h, \tag{1.64}$$

$$B = b, \tag{1.65}$$

and

$$C = -L. \tag{1.66}$$

Equation (1.62) then gives the critical value $d_{cr,4}$ as

$$d_{cr,4} = b\sin\theta^*_{cr,4} + L\cos\theta^*_{cr,4} - c. \tag{1.67}$$

In summary, Equations (1.43)-(1.55) are valid for $d_{cr,4} \le d \le d_{cr,3}$. If contact first occurs over this range, then the separation distance between the receptacle and pin at contact is

$$d_c = -c + \left(R + R_r\right)\sin\alpha_c + b\sin\theta_0 + L\cos\theta_0 \tag{1.68}$$

where

$$\alpha_c = \cos^{-1}\frac{L\sin\theta_0 - b\cos\theta_0 + h + e}{R + R_r}. \tag{1.69}$$

2.2.4. Receptacle on Pin Barrel

Figure 6 shows a geometric diagram for a receptacle arm in contact with a pin barrel. From the geometry of the problem, it is clear that when contact is established with the pin barrel, the angles and moment arms remain constant. Under the condition $d \ge d_{cr,4}$,

$$\theta^* = \theta^*_{cr,4} \tag{1.70}$$

and

$$\alpha = 0. \tag{1.71}$$

The moment arms are easily found from vector loop equation as

$$L_{mn} = L\cos\theta^* + b\sin\theta^* \tag{1.72}$$

and

$$L_{mt} = h - R_p \,. \tag{1.73}$$

In many situations, the receptacle stiffness is characterized via a finite element analysis in which the receptacle tip is flexed to a displacement commensurate with pin barrel contact. In this case, the force is often known and the effective spring stiffness needs to be found. To solve for the stiffness directly, (1.72) is substituted into (1.4), assuming static contact ($\mu = 0$), and rearranged to get

$$K = \frac{F_n}{\theta^*_{cr,3}}\left(L\cos\theta^*_{cr,3} + b\sin\theta^*_{cr,3}\right), \tag{1.74}$$

which can be approximated for small angles (using the first term of a series expansion) as

$$K \approx F_n L \tag{1.75}$$

in units of force times length per radian.

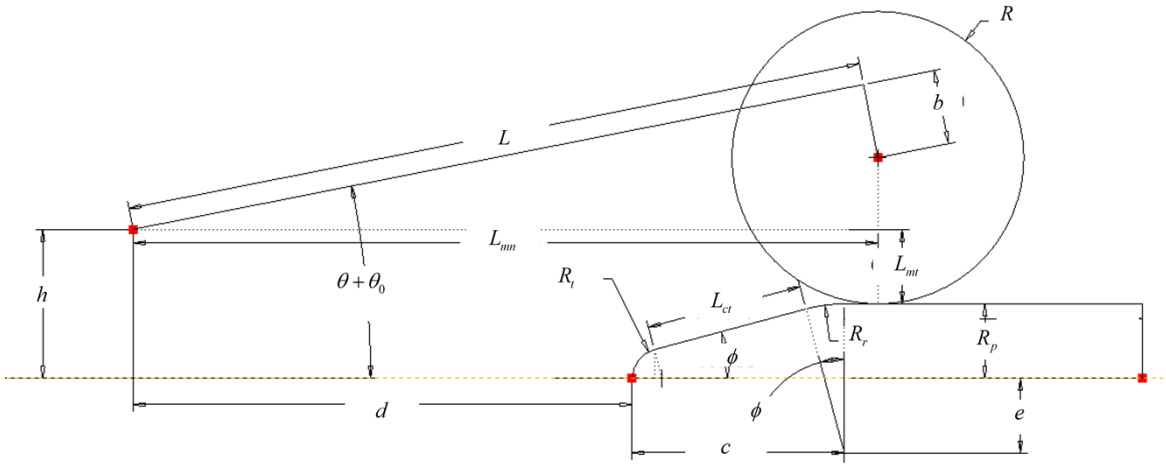

Figure 6. Geometric diagram for receptacle on pin barrel.

2.3. Geometric Compatibility

A number of geometric parameters were utilized to define the pin geometry, not all of which can be taken as independent. Based on the various geometric diagrams of Figure 3-Figure 6, some geometric compatibility equations can be found. Assuming the most relevant geometric parameters to be taken as inputs for the pin geometry are those likely to appear on a mechanical drawing (R_r, R_p, R_t, and ϕ), the geometric compatibility equations for the other parameters are

$$a = R_t \cos\phi\,, \tag{1.76}$$

$$e = R_r - R_p\,, \tag{1.77}$$

$$L_{ct} = \frac{R_r\cos\phi - (a+e)}{\sin\phi}\,, \tag{1.78}$$

and

$$c = R_t + \left(R_r - R_t\right)\sin\phi + L_{ct}\cos\phi\,. \tag{1.79}$$

where recall L_{ct} is the total cone length (along the cone).

2.4. Engagement vs. Disengagement

All equations presented thus far were derived for a receptacle moving in the $+x$ direction while engaging a pin. In instances where the receptacles disengage (circuit opens) as the mechanism moves, the receptacle disengages with the pin while moving in the $+x$ direction. In this case, shown in Figure 7, the bulk of the mathematical development remains unchanged but several equations must be modified.

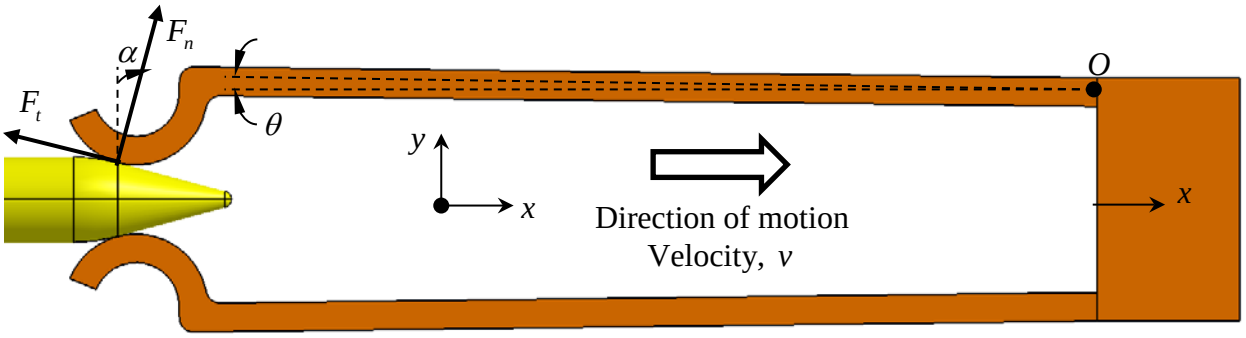

Figure 7. Simple example of receptacle-pin insertion.

First, the equation for separation distance, (1.8), becomes

$$d = d_0 + x\,, \tag{1.80}$$

because the separation distance increases from its initial value. In addition, the normal force expression, (1.4), becomes

$$F_n = \frac{K\theta}{L_{mn} + \mu L_{mt}} \tag{1.81}$$

due to the direction the friction acts for $+x$ motion. The resultant forces in the x-y coordinate system are then expressed as

$$F_x = F_n \sin\alpha - F_t \cos\alpha \tag{1.82}$$

and

$$F_y = F_n \cos\alpha + F_t \sin\alpha\,. \tag{1.83}$$

Equations (1.80) -(1.83) are the only ones that require modification to account for disengagement rather than engagement of the pin and receptacle with $+x$ motion.

2.5. Numerical Considerations

When using the contact model described herein as part of a larger dynamic model (for example, as one sub-function in an ODE solution), reversal of the friction force direction must be handled with care. A straightforward approach is the dynamic friction model (LMS, 2014),

$$\mu = \mu_{nom} \tanh\left(2.5\frac{v}{v_t}\right), \tag{1.84}$$

where μ_{nom} is the nominal coefficient of friction, $v = dx/dt$ is the relative velocity between the receptacle and pin, and v_t is a parameter known as transition velocity. The behavior of the anti-symmetric function (1.84) is shown in Figure 8. For a sufficiently small choice of v_t relative to typical velocities v, this model approximates static friction as well, with $\mu_s = \mu_{nom}$ (numerically, the goal is to be sure the receptacle moves so slowly that it may as well be still). Note that a similar approach is to let $\mu = \mu_{nom} \operatorname{sgn} v$, which is a piece-wise function defined as

$$\mu = \mu_{nom} \operatorname{sgn} v = \begin{cases} \mu_{nom} & v > 0 \\ 0 & v = 0 \\ -\mu_{nom} & v < 0 \end{cases}. \tag{1.85}$$

However, the discontinuous behavior of (1.85) at $v = 0$ is not friendly to many numerical algorithms. The approach of (1.84) is utilized in the Matlab code of Appendix B, with v / v_t taken as an input.

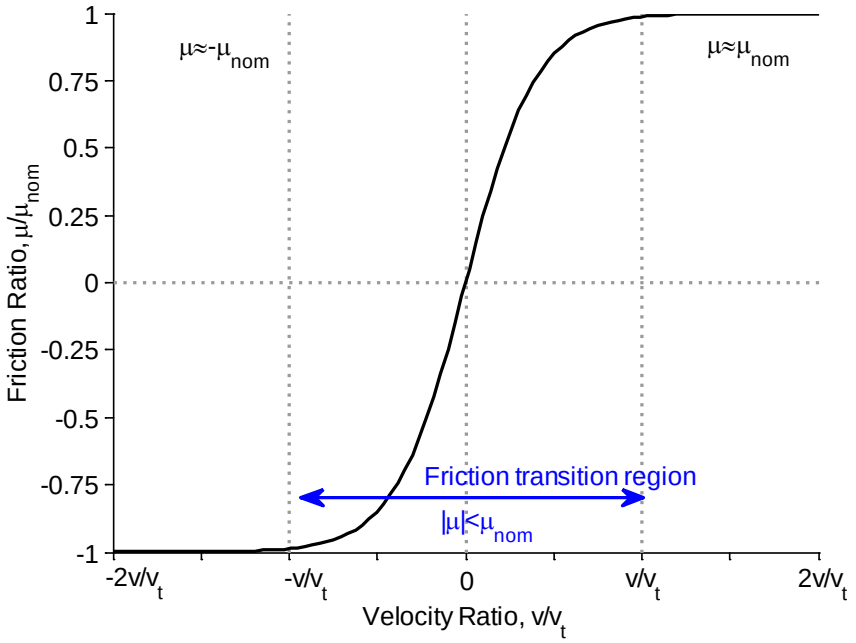

Figure 8. Dynamic friction model.

3. VALIDATION

3.1. Numerical

In this section, the Matlab implementation of the receptacle-pin contact model (see Appendix B) is validated against rigid body dynamics (RBD) simulations using LMS Virtual.Lab Motion (R13) for two nominal receptacle-pin geometries. In Section 3.1.1, the chosen geometry closely resembles the parameterized geometry used to develop the model (e.g. Figure 3-Figure 6). Both a nominal case and several variants are validated for this geometry. In Section 3.1.2, the robustness and flexibility of the contact model is demonstrated using a geometry that at first glance looks significantly different than the parameterized geometry

3.1.1. Bifurcated Receptacle

The RBD model for the nominal geometry under consideration is shown in Figure 9 in the un-deformed configuration. The overall RBD implementation is very similar to the analytical approach and utilizes many of the same assumptions. In particular, the receptacle arms are separated and rejoined at their base using revolute joints (single rotational degree of freedom, represented as green circles in Figure 9) with an associated torsional spring (represented as a blue spiral shape in Figure 9). The primary difference is that the contact is resolved directly from the solid geometry and that the simulation is dynamic (the arms possess inertia). This validation activity is primarily intended to show that the mathematical development is correct and that the Matlab code is free of errors. A more complete numerical validation exercise, for example using a finite element model with contact elements and an explicit-dynamic solution, is not pursued here. Even in the RBD context, the validity of the quasi-static nature of this model was not probed; the RBD model was configured to proceed from 0” to 0.210” and back again over 20s, with a maximum rate of ~0.031 in/s.

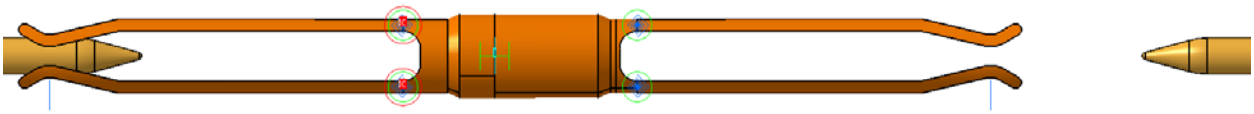

Figure 9. RBD model of receptacle-pin contact.

The nominal parameterized geometry used in the RBD model is shown in Figure 10. Other variants are also considered. Figure 10(a) shows the engaging side of the bifurcated receptacle and Figure 10 (b) shows the disengaging side (with +x motion). Although these receptacle-pin combinations are shown separately in Figure 10, they are rigidly connected as in Figure 9 and thus all results are given combined in plots. From the figure, the important parameters are extracted as given in Table 1. Of these, the pin and receptacle parameters are identical on both sides except for the initial offset distance d_0. Note also that the receptacle round center offset b is actually negative for this geometry because the round center is “above” the receptacle arm line (length L); in the derivation, the receptacle round center was “below” the receptacle arm line. A Matlab input deck consistent with Table 1 is found in Appendix B.

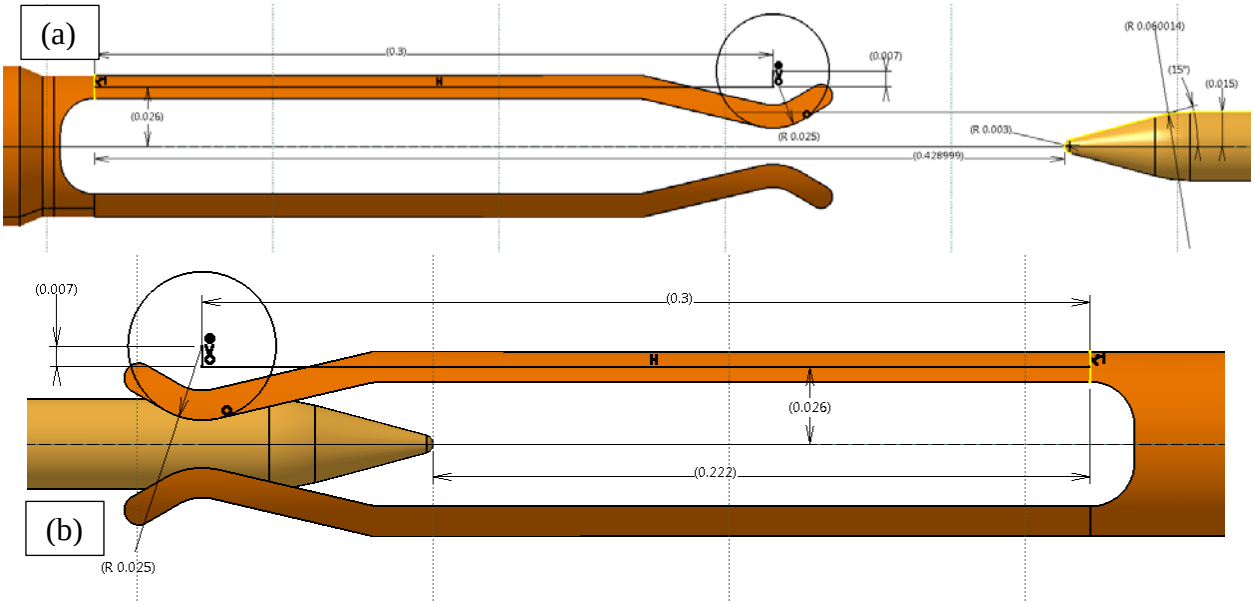

Figure 10. Validation case geometry (a) engaging with +x; (b) disengaging with +x.

Table 1. Input parameters for validation geometry 1.

Receptacle Arm Length, L	0.300”	
Receptacle Round Center Offset, b	-0.007”	
Receptacle Round Geometry, R	0.025”	
Receptacle Arm Height, h	0.026”	
Receptacle Arm Initial Angle, θ_0	0°	
Receptacle-Pin Initial Offset, d_0	0.429” Engaging, Figure 10(a)	0.222” Disengaging, Figure 10(b)
Receptacle Stiffness, K	0.004 lbf*in/deg	
Friction Coefficient, μ	0.020	
Pin Barrel Radius, R_p	0.015”	
Pin Cone Angle, ϕ	15°	
Pin Cone to Barrel Round Radius, R_r	0.060”	
Pin Tip Radius, R_t	0.003”	

Figure 11 shows the receptacle rotation predicted by the analytical code (solid line) and the RBD simulation (dots). The maximum rotation is ~1.336°. Note that there is no hysteresis in the receptacle rotation angle because it is uniquely defined by the location of contact on the pin for a given receptacle and pin geometry. Figure 12 shows the normal and tangential forces associated with the forward and reverse stroke, with excellent agreement between the analytical code and RBD. All force results are for a *single* receptacle arm. The dotted gray vertical lines represent the critical transitions. Proceeding from the left, these transitions are for contact at pin barrel-to-round and round-to-cone transitions (for the disengaging receptacle) and the cone-to-round and round-to-barrel transitions (for the engaging receptacle). Note that there is some hysteresis between the forward (+x) and reverse (-x) stroke for the normal and tangential forces. The magnitudes are slightly different depending on the direction of motion (the source of this is the

difference in denominator sign between (1.4) or (1.81)), but the hysteresis is driven by the change in direction of the force (see the tangential force F_t). Figure 13 shows the x- and y-direction forces associated with the forward and reverse strokes. The x-direction force F_x is the insertion force and has the most interesting hysteretic behavior driven by the changing contributions of the normal and tangential forces as the receptacle negotiates the pin from cone to barrel. For the full insertion force associated with the entire receptacle pictured in Figure 9, the insertion force plotted in Figure 13 can be multiplied by 2 (for two receptacle arms per side). Figure 14 shows the normal and tangential moment arms, L_{mn} and L_{mt}, respectively. This plot is slightly different than the others in that the moment arms are shown even for displacement at which the receptacle would be required to bend *toward* the pin in order to make contact. As expected, $L_{mn} \approx L$ and $L_{mt} = h - R_p$ when the receptacle is in contact with the pin barrel.

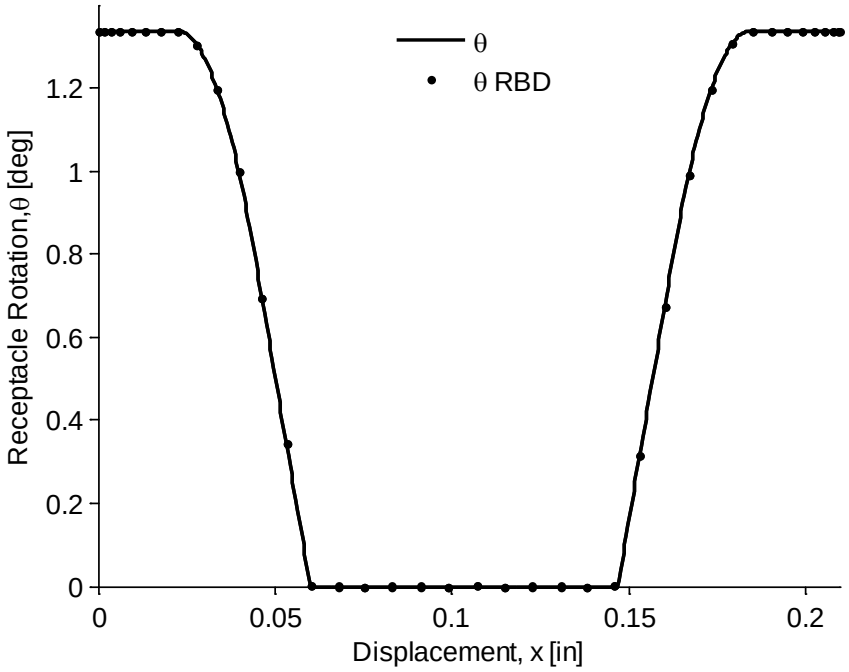

Figure 11. Receptacle arm rotation for nominal validation case.

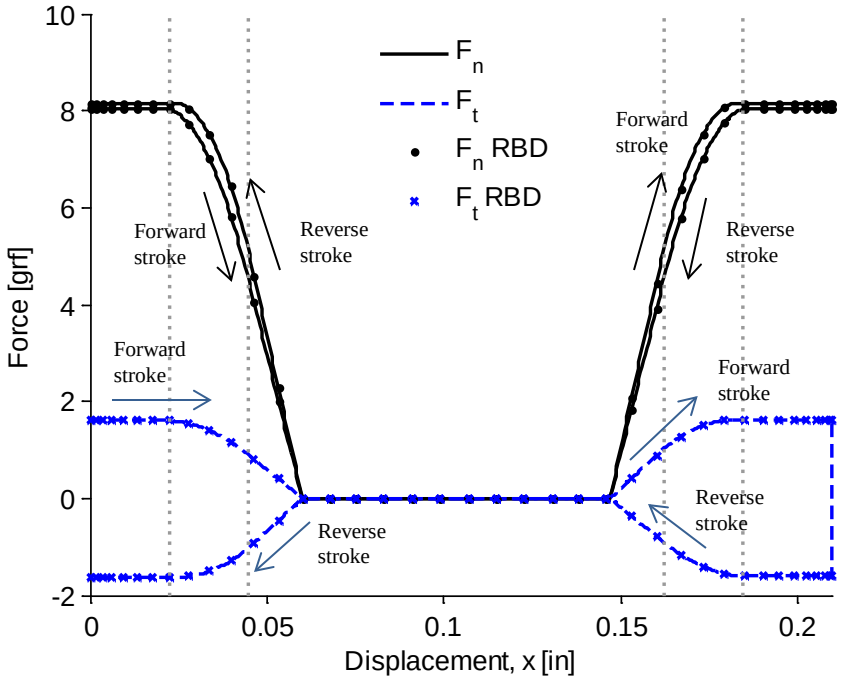

Figure 12. Normal and tangential forces for nominal validation case (single receptacle arm).

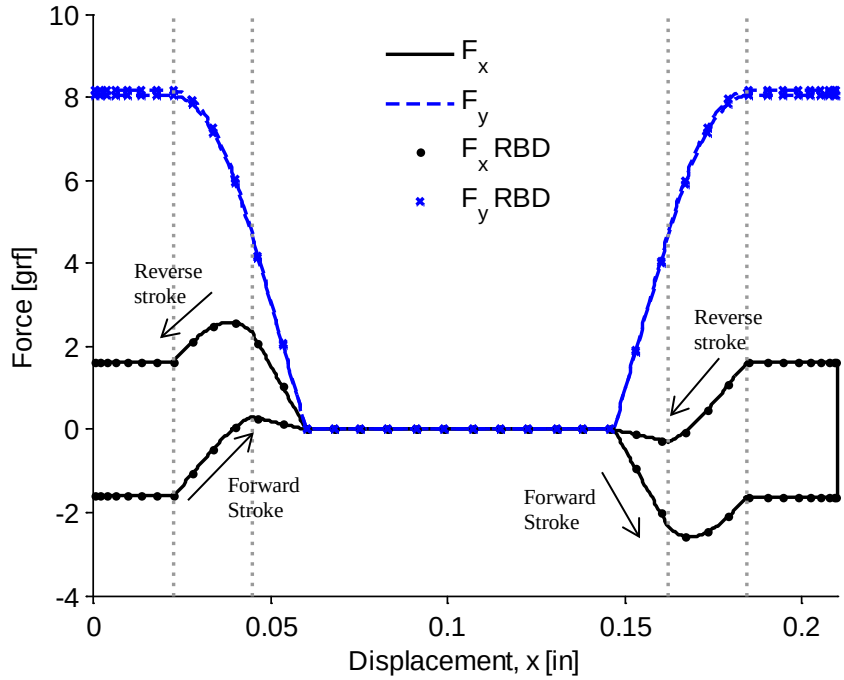

Figure 13. X- and Y-direction forces for nominal validation case (single receptacle arm).

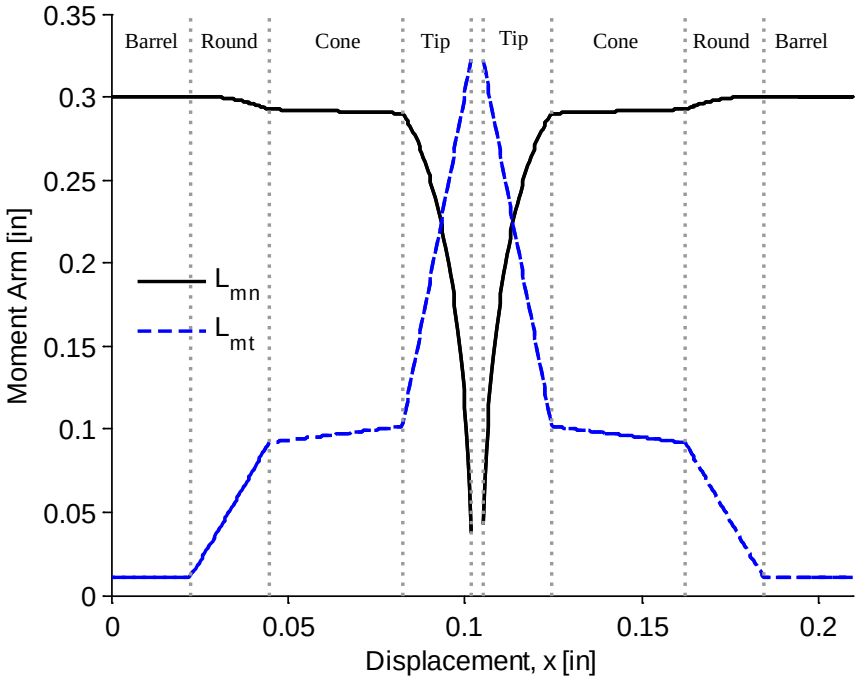

Figure 14. Normal and tangential moment arms.

Next, some parameter excursions from the nominal geometry are examined, with the focus on initial imperfection θ_0 , friction coefficient μ , and pin angle ϕ . For each parameter sweep, the insertion force F_x is evaluated in both the analytical Matlab code and in the RBD model. Figure 15 shows the results when an initial imperfection θ_0 from -0.5° to 0.5°. One result is that the displacement at which contact occurs moves (contact occurs over a larger portion of the stroke for negative θ_0 and a smaller portion of the stroke for positive θ_0). The peak contact forces also chane; they are larger for smaller θ_0 because the receptacle arm must effectively flex by the additional amount θ_0. RBD simulation results are plotted for three of the cases (black dots) and agree very closely. Figure 16 shows the results when the friction coefficient is varied, with $\mu = \{0, 0.1, 0.2, 0.35, 0.5\}$. As μ increases, the magnitude of the insertion force as well as the hysteresis increases substantially as expected. RBD simulation results (black dots) are included for the $\mu = \{0, 0.2, 0.5\}$ cases with excellent agreement. Finally, pin geometries with $\phi = \{10°, 15°, 30°\}$ were simulated, with the pins depicted in Figure 17(a-c). Because the pin cone-to-barrel transition round remained unchanged, the peak insertion force in Figure 18 was the same for each simulation, though the portion of the stroke over which contact occurred did change. The RBD simulations again agreed extremely closely with the Matlab results.

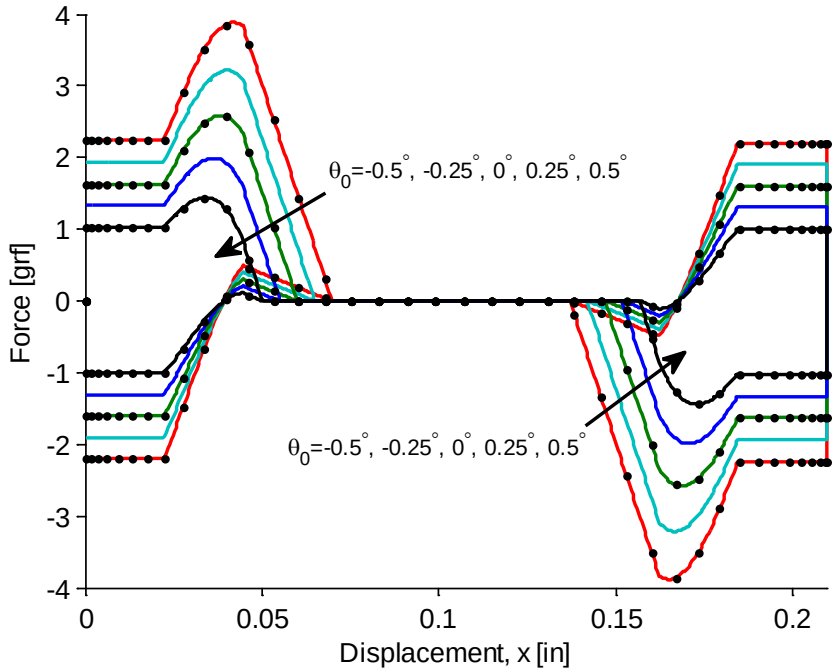

Figure 15. Analytical predictions of insertion force (F_x) for various initial imperfections (lines) compared to RBD results for the same (dots).

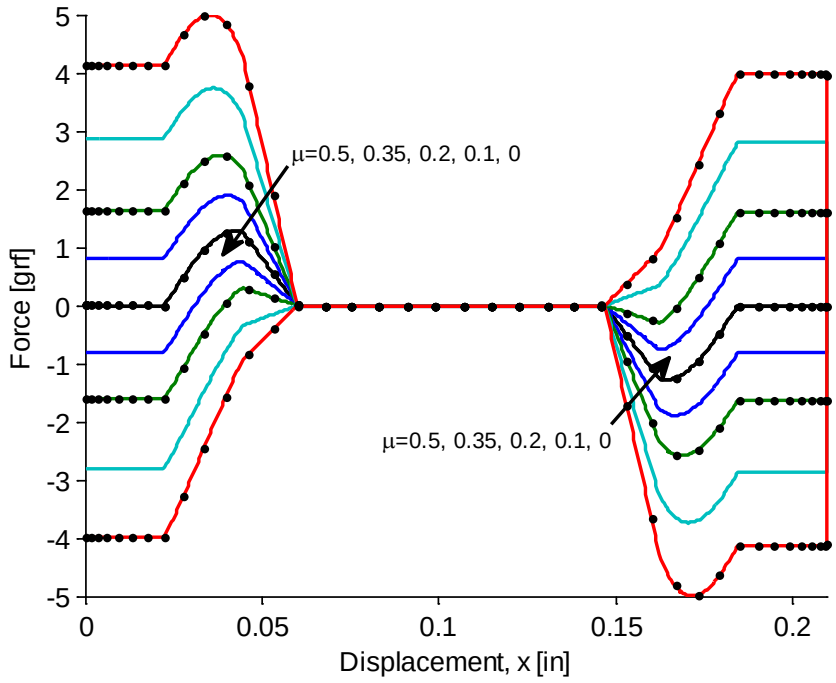

Figure 16. Analytical predictions of insertion force (F_x) for various friction coefficients (lines) compared to RBD results for the same (dots).

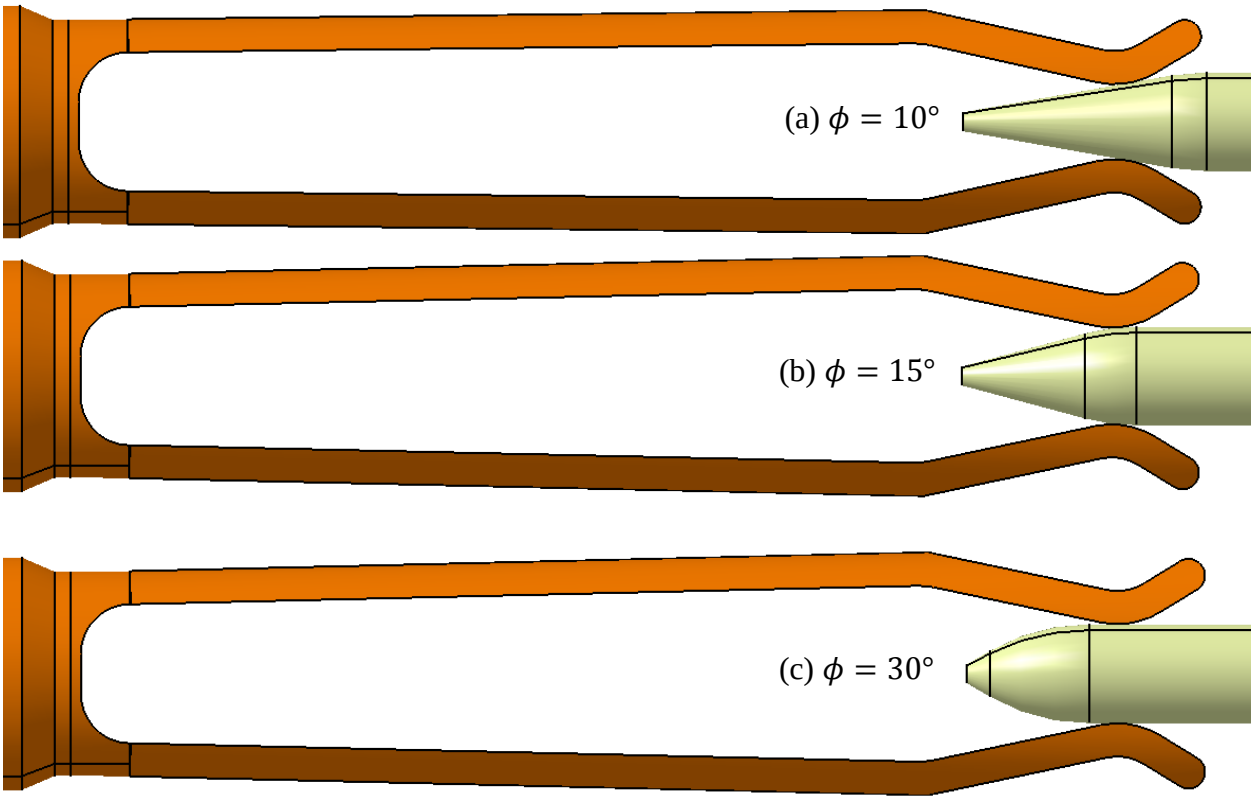

Figure 17. Pin geometry study with ϕ= (a) 10° ; (b) 15°; (c) 30°.

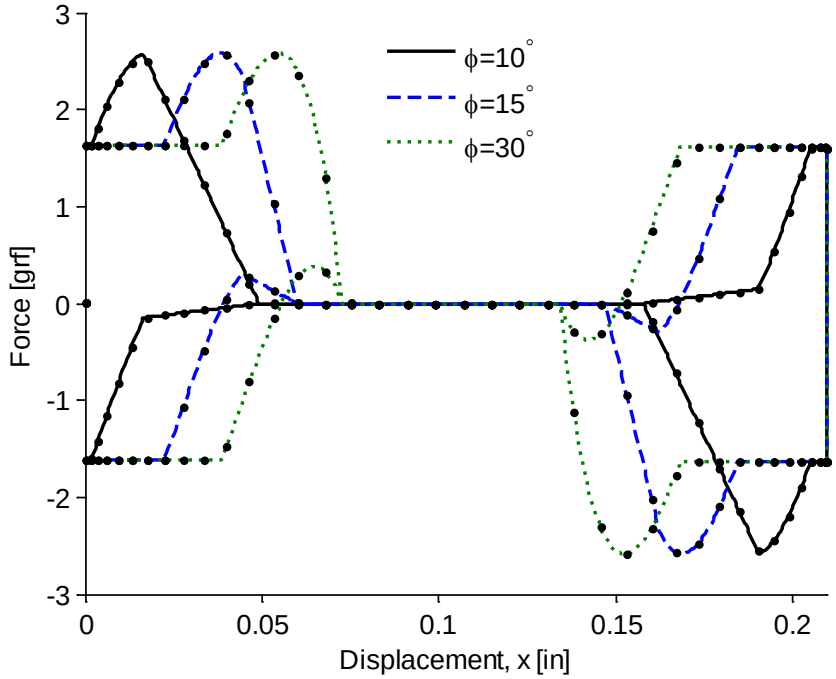

Figure 18. Analytical predictions of insertion force for various pin cone angles (lines) compared to RBD results for the same (dots).

3.1.2. Flexure and Round-Headed Pin

The geometry under consideration in this section is shown in Figure 19 (screenshot from RBD with a revolute joint represented by a green circle and a torsion spring shown as a blue spiral). Here, a single blade flexure makes contact with a round-headed pin. This geometry does not at first glance seem to resemble the parameterized geometry used in model development; in particular, the flexure contact area actually trails the pivot, and the pin has no "cone" feature. It is shown in this section that the model is fully capable of predicting contact forces for this case.

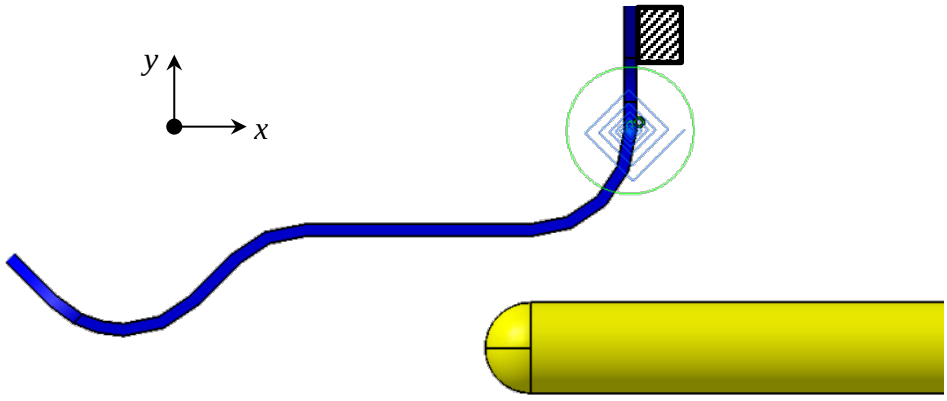

Figure 19. Flexure and round-headed pin.

The key to determining the geometric parameters appropriate for this geometry is to make it appear like the geometry used in model development. Figure 20 shows a sketch overlaying the flexure geometry and another version (toward the right) rotated 180° such that the contact circle is in the +x direction from the receptacle flexure point. Referencing this latter image makes it straightforward to determine the various geometric parameters and then the flexure may be specified in the correct orientation using $\theta_0 = \pm 180°$. Table 2 collects the model input parameters from Figure 20. Some particular dimensions to note are b (negative because it extends away from the pin), d_0 (negative because the receptacle rotation point is in the +x direction relative to the pin tip), and the fact that $R_t = R_r = R_p$ with $\phi = 45°$. This latter set of dimensions effectively splits the single pin tip radius (0.015") between the original pin tip in the derivation (R_t) and the cone-to-barrel transition round (R_r) while collapsing the length of the cone to zero at an arbitrary point ($\phi = 45°$) along the curve. Note that the sub-mil decimal places found in some dimensions within Table 2 are not necessary for a good solution; they are just included for consistency with Figure 20. A Matlab input deck consistent with Table 2 is found in Appendix B.

Figure 21-Figure 24 collect the predicted receptacle arm rotation, normal/tangential forces, x- and y-direction forces, and moment arms, respectively. Vertical gray dotted lines on the plots show critical values of the displacement, x. These results are compared to the RBD model prediction for a dynamic simulation featuring an excursion from $x = 0$ to $x = 0.2"$ and back again over 10 s, with a transition velocity of 1e-3 in/s. This shows the model (and Matlab implementation) are very flexible and robust.

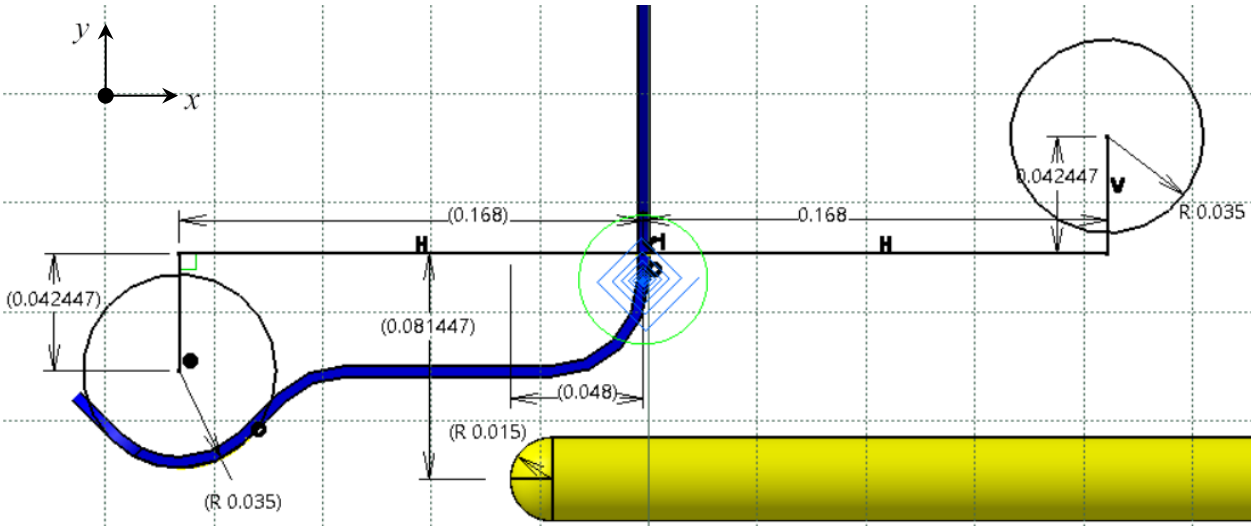

Figure 20. Flexure and round-headed pin geometry parameterization.

Table 2. Input parameters for single-sided receptacle geometry.

Receptacle Arm Length, L	0.168”
Receptacle Round Center Offset, b	-0.042447”
Receptacle Round Geometry, R	0.035”
Receptacle Arm Height, h	0.081447”
Receptacle Arm Initial Angle, θ_0	±180° (180° selected)
Receptacle-Pin Initial Offset, d_0	-0.048”
Receptacle Stiffness, K	0.00067 lbf*in/deg
Friction Coefficient, μ	0.020
Pin Barrel Radius, R_p	0.015”
Pin Cone Angle, ϕ	$\phi \in (0°,90°)$; 45° selected
Pin Cone to Barrel Round Radius, R_r	0.015”
Pin Tip Radius, R_t	0.015”

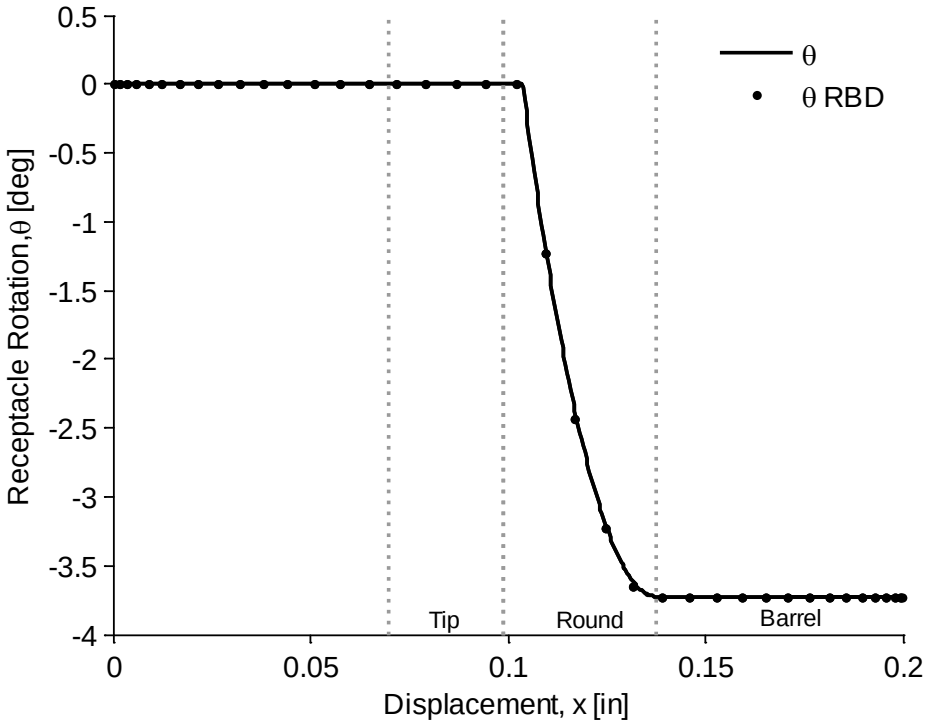

Figure 21. Flexure rotation angle.

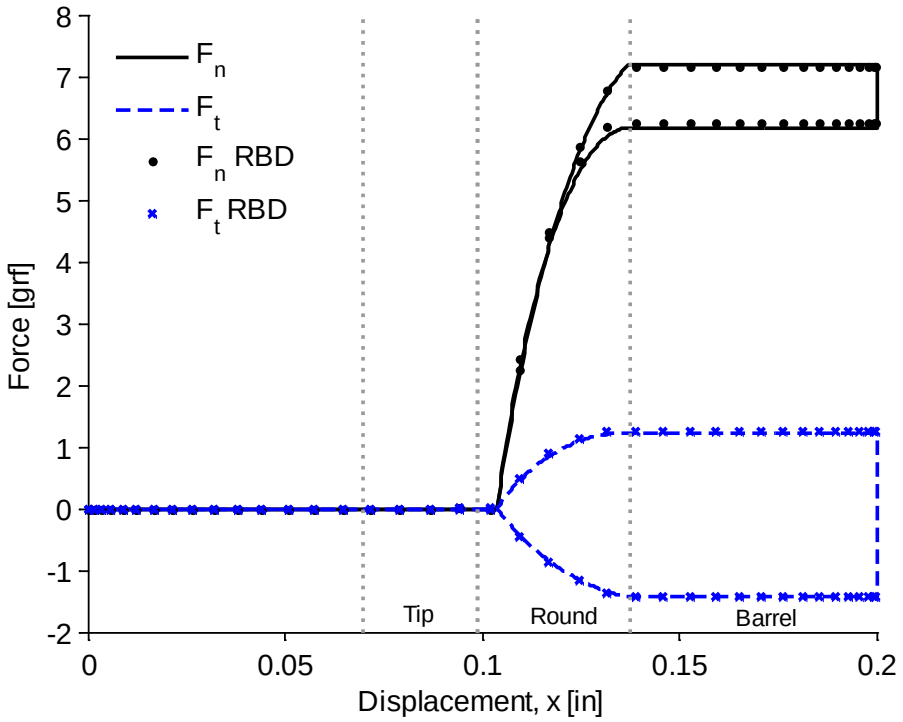

Figure 22. Normal and tangential forces between the flexure and round-headed pin.

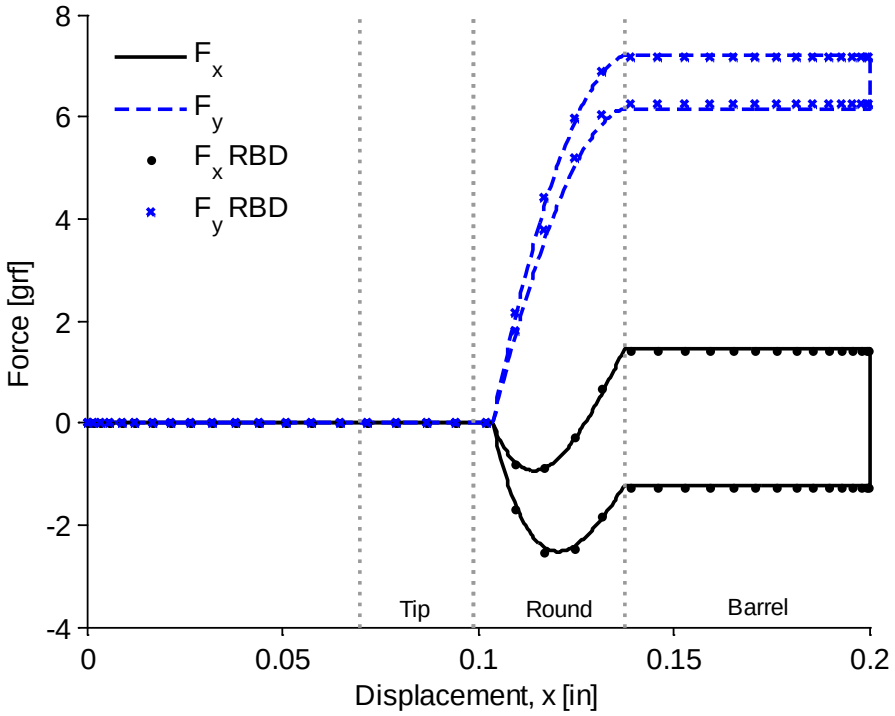

Figure 23. X- and Y-direction forces for the flexure and round-headed pin.

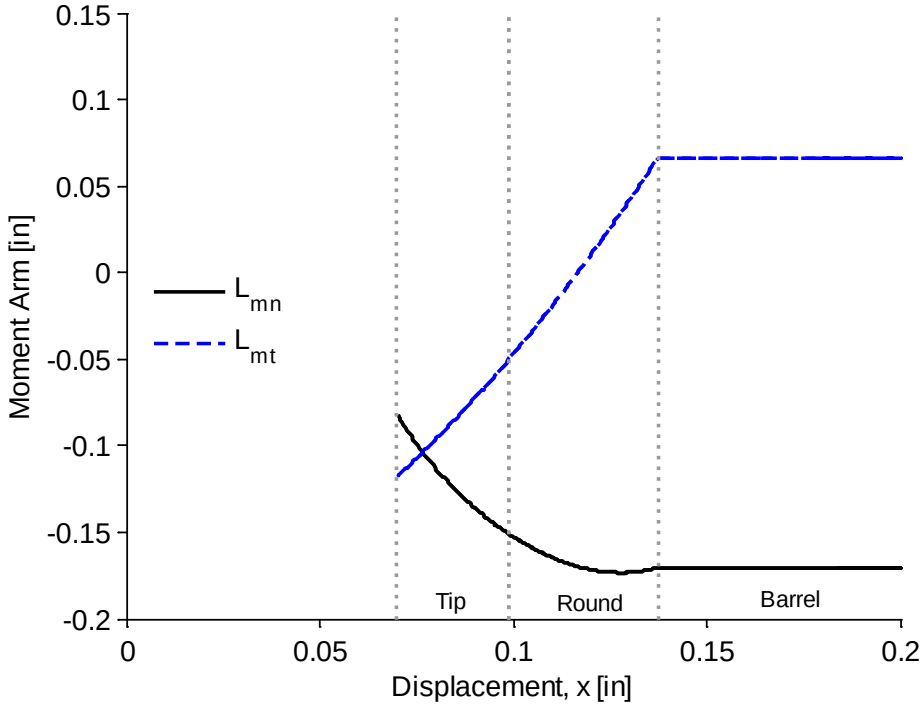

Figure 24. Normal and tangential moment arms for the flexure and round-headed pin.

3.2. Experimental

In 2011, an experimental study was conducted (Sena 2012) to determine the insertion force and contact resistance for the receptacle design nominally depicted in Figure 25 ($L = 0.316"$, $h = 0.0375"$, $b = 0.0045"$, and $R = 0.025"$). The pin geometry was the same as depicted in Figure 10(a). The test setup featured a 25 gram load cell and precision stages to control alignment as well as to engage the receptacle with the pin.

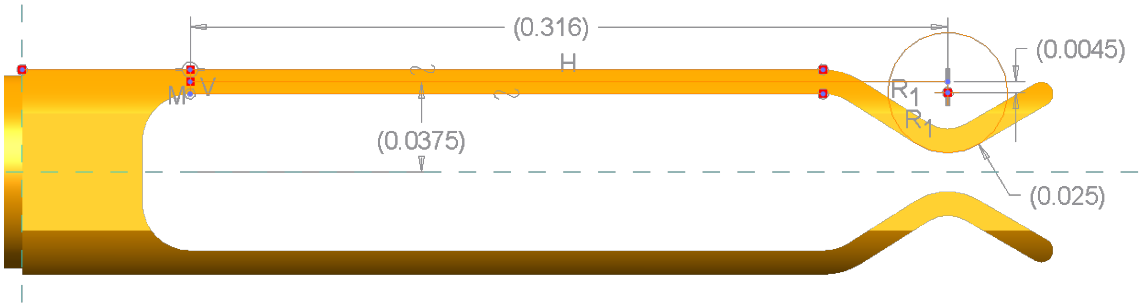

Figure 25. Nominal receptacle arm geometry used in insertion force measurements.

Using the nonlinear greybox modeling and parameter extraction capabilities of the Matlab System Identification Toolbox, the receptacle-pin contact model was tuned to a set of experimental data. For simplicity, the free parameters were limited to the initial separation distance d_0, the receptacles stiffness K, and the friction coefficient μ and those parameters were found to be 0.369", 0.0116 lbf*in/deg, and 0.21, respectively. Figure 26 shows the model overlaid with experimental data for five insertions of the receptacle onto the pin. Ripples in the experimental data are of course not captured, but the shape of the forward and reverse stroke, as well as the magnitude of the force, agrees very well. This shows that the receptacle-pin contact model is fundamentally valid for estimating the insertion force to acceptable accuracy.

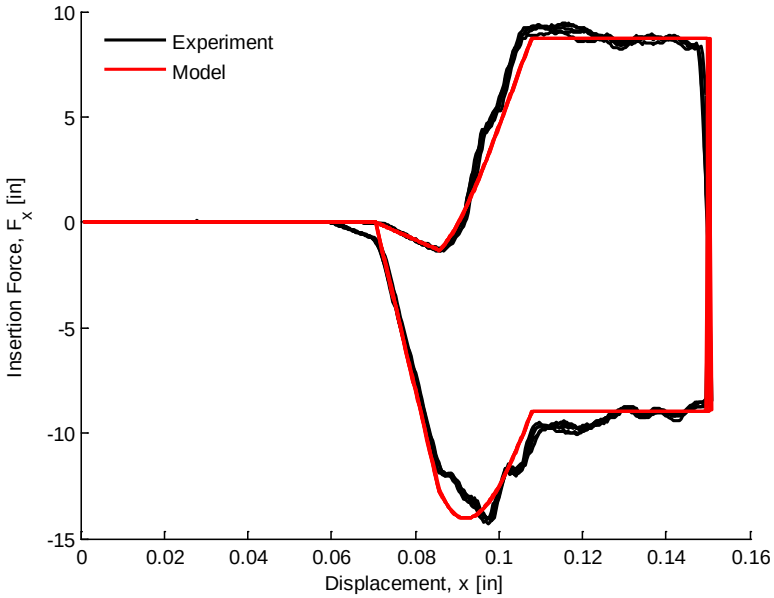

Figure 26. Comparison of insertion force from experiment and simulation.

4. CONCLUSIONS

A closed-form, quasi-static receptacle-pin contact model was developed with the primary goal being the determination of the insertion force associated with a bifurcated receptacle (or other related geometry) being engaged with a pin. The model geometry and other inputs were parameterized to allow predictions of forces for different geometries, friction coefficients, receptacle stiffnesses, etc. A receptacle angular imperfection parameter was also included.

A Matlab implementation of the model is supplied in Appendix B, and was written so that it can be utilized as a sub-function in reduced-order, ODE-based models of mechanisms. The model implementation was validated against a typical RBD model of a bifurcated receptacle negotiating a pin as well as a flexure arm in contact with a round-headed pin. In addition, the model was compared to experimental measurements of insertion force for yet another receptacle design. The model agreed extremely closely with the RBD model results, showing the underlying mathematics and code implementation were approached correctly. Agreement with experimental results was also very good, showing that the model does a good job capturing the characteristics of the insertion force. Overall, the model is simple and efficient to use for electrical contact geometries similar to those demonstrated herein.

For future work, a similar overall approach could be used to include imperfection in the pin orientation, though the mathematics would be significantly more difficult. Another extension that could add value would be linearization of many of the equations herein about $\theta = \theta_0$, which could potentially eliminate the need to utilize the quadratic equation to find θ. With the quadratic equation no longer required, the nuances of choosing the correct solution would also be eliminated. This route was not taken because the Matlab code in its current form was shown to work well for a variety of receptacle and pin geometries.

5. REFERENCES

Larry L. Howell, 2001, *Compliant Mechanisms*, Wiley, New York, NY.

LMS, LMS Virtual.Lab Motion Help File. Topic: Friction.

Michael P. Sena, October 18, 2012 *Electrical Contact Comparison*, presentation, SNL.

APPENDIX A: CLOSED-FORM SOLUTION TO TRIG EQUATION

Equations in this report were frequently put in the form

$$A + B\cos\theta^* + C\sin\theta^* = 0, \tag{1.86}$$

which may be solved in closed-form. Using well-known trig identities

$$\cos\theta^* = \frac{1-\tan^2\frac{\theta^*}{2}}{1+\tan^2\frac{\theta^*}{2}} \tag{1.87}$$

and

$$\sin\theta^* = \frac{2\tan\frac{\theta^*}{2}}{1+\tan^2\frac{\theta^*}{2}}, \tag{1.88}$$

the solution to this equation can be found as

$$\tan\frac{\theta^*}{2} = \frac{-C \pm \sqrt{C^2 - \left(A^2 - B^2\right)}}{A - B}. \tag{1.89}$$

Clearly, for a real root to exist,

$$C^2 \geq \left(A^2 - B^2\right). \tag{1.90}$$

The solution for θ, utilizing (1.7), is then

$$\theta = 2\tan^{-1}\left(\frac{-C \pm \sqrt{C^2 - \left(A^2 - B^2\right)}}{A - B}\right) - \theta_0. \tag{1.91}$$

The two solutions correspond to the one of interest (in which the receptacle arm has displaced slightly from its free position) and one in which the receptacle arm has rotated approximately 180º. Following some investigation, the best indicator for selecting the correct root was found to be the sign of C and $\cos\theta_0$. Letting

$$n = \mathrm{sgn}\left(C\cos\theta_0\right), \tag{1.92}$$

the final equation that selects the correct root is then

$$\theta = 2\tan^{-1}\left(\frac{-C + n\sqrt{C^2 - \left(A^2 - B^2\right)}}{A - B}\right) - \theta_0. \tag{1.93}$$

APPENDIX B: MATLAB CODES

Main Function: rec_pin_contact.m

```
function [Fx,Fy,Fn,Ft,theta,Lmn,Lmt, dcr,thetacr,xcr,dc,xc]=...
      rec_pin_contact(x,params,vnorm,dir,d0);
% [Fx,Fy,Fn,Ft]=rec_pin_contact(x,params,vnorm,dir) returns the
% various forces associated with a single receptacle arm to pin contact. Fx
% is the force in the x-direction (direction of motion), Fy is the force
% perpendicular to Fx, Fn is the normal force, and Ft is the tangential
% (friction) force. The force vectors satisfy the relationship
% norm([Fx,Fy])=norm([Fn,Ft]) since the magnitude must remain the same
% regardless of coordinate system. The inputs are the displacement of the
% piston (x, which may be an array), parameters associated with the pin and
% contact (params), the normalized velocity (velocity divided by transition
% velocity, which must be the same size as x), and dir is either
% 'engage' (or +1) or 'disengage' (or -1) depending on which behavior
% occurs with +x motion.  List of fields that must be included within the
% input params, where [L] and [F] denote arbitrary consistent length and
% force units, respectively:
%
%   Rr = Pin cone-to-barrel round radius [L]
%   Rp = Pin barrel radius [L]
%   phi = Pin cone angle (relative to axis) [deg]
%   Rt = Pin tip radius [L]
%
%   h = Height from pin axis to receptacle rotation point [L]
%   R = Receptacle contact radius [L]
%   L = Receptacle arm length [L]
%   b = Perpendicular distance from receptacle arm to R center [L]
%   K = Angular stiffness [F*L/deg]
%   mu = Friction coefficient [-]
%   d0 = Initial separation distance from receptacle pivot to pin tip [L]
%   theta0 = Imperfection angle [deg]
%
% [Fx,Fy,Fn,Ft,theta,Lmn,Lmt,dcr,thetacr,xcr,dc,xc]=rec_pin_contact(...);
% yields additiona outputs:
%   theta = Receptacle rotation angle [rad]
%   Lmn = Normal force moment arm [L]
%   Lmt = Tangential force moment arm [L]
%   dcr = Critical separation distances [L]
%   thetacr = Critical receptacle arm rotations [rad]
%   xcr = Critical displacements [L]
%   dc = Separation distance at first contact [L]
%   xc = Displacement at first contact [L]
%
% [...]=rec_pin_contact(x,params,vnorm,dir,d0) ignores any value given in
% params.d0 and uses the final input argument d0 instead.  This mode is
% useful if a set of engaging and disengaging receptacles and pins are
% geometrically the same, enabling a single structure params to be used
% with two function calls.  Giving vnorm=[] and/or dir=[] reverts to
% defaults for those inputs.

%% Inputs %%%%%%%%%%%%%%%%%%%%%%%%%%%%%%%%%%%%%%%%%%%%%%%%%%%%%%%%%%%%%%%%%%%
```

```
% Defaults
if nargin<5 % If d0 not given explicitly, use value in params
   d0=params.d0;
end % Otherwise d0 is as given
if nargin<4|isempty(dir) % If dir not given or given as empty
    try
        dir=params.dir; % Look for value stored in params
    catch
        dir=1; % Default to +1 (same as 'engage') otherwise
    end
end
if nargin<3|isempty(vnorm) % If vnorm not given or given as empty
    vnorm=10*ones(size(x)); % Default to 10 for all values of x
end

% Pin Parameters
Rr=params.Rr; % Pin round (ramp to barrel) [L]
Rp=params.Rp; % Pin barrel radius [L]
phi=params.phi*pi/180; % Pin cone angle: Given in [deg], converted to [rad]
Rt=params.Rt; % Pin tip radius [in]

% Contact parameters
h=params.h; % Height from pin axis to receptacle rotation point [L]
R=params.R; % Round of receptacle contact [L]
b=params.b; % Perpendicular distance from receptacle arm end to R center [L]
L=params.L; % Receptacle arm length [L]
K=params.K*180/pi; % Angular stiffness [F*L/deg] to [F*L/rad]
mu=params.mu; % Friction coefficient [-]
theta0=params.theta0*pi/180; % Receptacle imperfection [deg] to [rad]

%% Calculate Additional Pin Geometric Parameters %%%%%%%%%%%%%%%%%%%%%%%%%%
a=Rt*cos(phi); % Pin tip "flat" dimension [in]
e=Rr-Rp; % Equation (1.77), [in]
Lct=(Rr*cos(phi)-(a+e))/sin(phi); % Equation (1.78)
c=Rt+(Rr-Rt)*sin(phi)+Lct*cos(phi); % Equation (1.79)

%% Solution Frame %%%%%%%%%%%%%%%%%%%%%%%%%%%%%%%%%%%%%%%%%%%%%%%%%%%%%%%%

% Calculate Critical Points %
% The following code calculates critical transition points for both the
% receptacle rotation (thetacr [rad]) and piston displacement (dcr
% [in]).
% Index 1 : Tip
% Index 2 : Tip to ramp
% Index 3 : Ramp to round
% Index 4 : Round to barrel

A=-h; B=b; C=-L;
thetacr(1)=eqnsol(A,B,C,theta0); % Equation (1.22)

A=-h+(Rt+R)*cos(phi); B=b; C=-L;
thetacr(2)=eqnsol(A,B,C,theta0); % Equation (1.24)

A=(R+Rr)*cos(phi)-(h+e); B=b; C=-L; % Equations (1.58)-(1.60)
thetacr(2)=eqnsol(A,B,C,theta0); % Solution of Equation (1.57)
```

```
A=R+Rp-h; B=b; C=-L; % Equations (1.64)-(1.66)
thetacr(4)=eqnsol(A,B,C,theta0); % Solution of (1.63)

alphacr=[pi/2,phi];
dcr(1:2)=-Rt+(R+Rt)*sin(alphacr)+b*sin(thetacr(1:2)+theta0)+ ...
    L*cos(thetacr(1:2)+theta0); % Equation (1.9) in lieu of (1.23) & (1.25)
alphacr=[phi,0];
dcr(3:4)=(L*cos(thetacr(3:4)+theta0)+b*sin(thetacr(3:4)+theta0) ...
    +(R+Rr)*sin(alphacr)-c); % Equation (1.43) in lieu of (1.61) & (1.62)

% Find separation distance at contact
dc(1)=-Rt+(Rt+R)*sin(acos((L*sin(theta0)-b*cos(theta0)+h)/(Rt+R)))+ ...
    b*sin(theta0)+L*cos(theta0); % Equations (1.27) and (1.28)
dc(2)=-Rt+Rt*sin(phi)-(h-a-R*cos(phi)-b*cos(theta0)+L*sin(theta0))/...
    sin(phi)*cos(phi)+R*sin(phi)+b*sin(theta0)+...
    L*cos(theta0); % Equations (1.41) & (1.42)
dc(3)=-c+(R+Rr)*sin(acos((L*sin(theta0)-b*cos(theta0)+h+e)/(R+Rr)))+ ...
    b*sin(theta0)+L*cos(theta0); % Equations (1.68) and (1.69)
dm=[dcr(1),dcr(2),dcr(3);
    dcr(2),dcr(3),dcr(4)];
dc=dc(dc<dm(1,:)&dc>=dm(2,:)); % Choose single correct dc value

% The relationship between displacement (x) and initial separation (d0) is
% different depending on if the receptacle is engaging or disengaging w/ +x
% motion.
switch dir
    case {'engage',1}
        d=d0-x; % Equation (1.8)
        xcr=d0-dcr; % Critical displacements via form of Equation (1.8)
        xc=d0-dc; % Displacement at contact via form of Equation (1.8)
    case {'disengage',-1}
        d=d0+x; % Equation (1.80)
        xcr=dcr-d0; % Critical displacements via form of Equation (1.80)
        xc=dc-d0; % Displacement at contact via form of Equation (1.80)
end

% Initializations %
theta=zeros(size(x)); % Initialize receptacle arm rotation [rad]
alpha=zeros(size(x)); % Initialize pin surface normal angle [rad]
Lmn=inf*ones(size(x)); % Initialize normal force moment arm [in]
Lmt=inf*ones(size(x)); % Initialize friction force moment arm [in]
m=sign(cos(theta0)); % Used in forms of Equation (1.26)

% Calculations %
% Now calculate moment arms, contact angles, receptacle rotation, etc. for
% every value of x (d).

% On Tip %
I=d<=dcr(1)&d>dcr(2);
A=L^2+b^2+h^2+(Rt+d(I)).^2-(Rt+R)^2; % Equation (1.14)
B=-2*(L*(Rt+d(I))+b*h); % Equation (1.15)
C=2*(L*h-b*(Rt+d(I))); % Equation (1.16)
th=eqnsol(A,B,C,theta0); % Solve Equation (1.12)
al=acos((L*sin(th+theta0)-b*cos(th+theta0)+h)/(Rt+R)); % Equation (1.17)
Lmn(I)=(Rt+d(I)).*cos(al)-h*sin(al); % Equation (1.20)
Lmt(I)=(Rt+d(I)).*sin(al)+h*cos(al)-Rt; % Equation (1.21)
```

```
theta(I)=max(theta(I),m*th)*m; % Equation (1.26) to select 0 or th
alpha(I)=al;

% On Ramp %
I=d<=dcr(2)&d>dcr(3);
A=d(I)+Rt-(Rt+R)*sin(phi)+((h-a)-R*cos(phi))/tan(phi); % Equation (1.33)
B=-b/tan(phi)-L; % Equation (1.34)
C=L/tan(phi)-b; % Equation (1.35)
th=eqnsol(A,B,C,theta0); % Solution to Equation (1.32)
Lc=(-b*cos(th+theta0)+L*sin(th+theta0)-R*cos(phi)+(h-a))/...
    sin(phi); % Equation (1.31)
Lmn(I)= (d(I)+Rt-Rt*sin(phi))*cos(phi)-(h-a)*sin(phi) + Lc; % Equation (1.38)
Lmt(I)= (d(I)+Rt)*sin(phi)+(h-a)*cos(phi) + Rt*cos(phi)^2-Rt; % Eq. (1.39)
theta(I)=max(theta(I),th*m)*m; % Equation (1.26) to select 0 or th
alpha(I)=phi; % Equation (1.40)

% On Round %
I=d<=dcr(3)&d>dcr(4);
A=(R+Rr)^2-L^2-b^2-(d(I)+c).^2-(h+e)^2; % Equation (1.48)
B=2*L*(d(I)+c)+2*b*(h+e); % Equation (1.49)
C=2*b*(d(I)+c)-2*L*(h+e); % Equation (1.50)
th=eqnsol(A,B,C,theta0); % Solve equation (1.47)
al=acos((-b*cos(th+theta0)+L*sin(th+theta0)+(h+e))/(R+Rr)); % Equation (1.51)
Lmn(I)=(d(I)+c).*cos(al)-(h+e).*sin(al); % Equation (1.54)
Lmt(I)=(d(I)+c).*sin(al)+(h+e).*cos(al)-Rr; % Equation (1.55)
theta(I)=max(theta(I),th*m)*m; % Equation (1.26) to select 0 or th
alpha(I)=al;

% On Barrel %
I=d<=dcr(4);
theta(I)=max(theta(I),thetacr(4)*m)*m; % Eq. (1.26) to select 0 or Eq. (1.70)
alpha(I)=0; % Equation (1.71)
Lmn(I)=L*cos(theta(I)+theta0)+b*sin(theta(I)+theta0); % Equation (1.72)
Lmt(I)=h-Rp; % Equation (1.73)

% Forces %
% Dynamic friction coefficient (98% of +/-mu at vnorm=+/-1), Equation (1.84)
mud=mu*tanh(2.5*vnorm);
% Directionality of friction affects everything starting from the magnitude
% of Fn and propagating through to Fx and Fy. The switch as well as the
% dynamic friction coefficient (mud) below accounts for this.
switch dir
    case {'engage',1}
        Fn=K*theta./(Lmn-mud.*Lmt); % Equation (1.4)
        Fn(isinf(Lmn))=0;
        Ft=mud.*Fn; % Equation (1.3)
        Fx=-Fn.*(sin(alpha)+mud.*cos(alpha)); % Equation (1.5)
        Fy=Fn.*(cos(alpha)-mud.*sin(alpha)); % Equation (1.6)
    case {'disengage',-1}
        Fn=K*theta./(Lmn+mud.*Lmt); % Equation (1.81)
        Fn(isinf(Lmn))=0;
        Ft=mud.*Fn; % Equation (1.3)
        Fx=Fn.*(sin(alpha)-mud.*cos(alpha)); % Equation (1.82)
        Fy=Fn.*(cos(alpha)+mud.*sin(alpha)); % Equation (1.83)
end
```

```
function val=eqnsol(A,B,C,theta0)
% Solve Equation (1.86) and select correct root
n=sign(C)*sign(cos(theta0)); % Equation (1.92)
val=wrap(2*atan((-C+n.*sqrt(C.^2-(A.^2-B.^2)))./ ...
    (A-B))-theta0); % Equation (1.93)

function val=wrap(valin);
% Wrap to [-pi,pi] interval
val=mod(valin,2*pi);
j=val>pi; val(j)=val(j)-2*pi;
j=val<-pi; val(j)=val(j)+2*pi;
```

Input Deck: Bifurcated Receptacle

```
%% Bifurcated Receptacle
close all
clear all

%% Define Pin and Receptacle Geometry
params.Rr=0.06; % Pin round (ramp to barrel) [in]
params.Rp=0.015; % Pin barrel radius [in]
params.phi=15; % Pin ramp angle (pin axis to ramp) [deg]
params.Rt=.003; % Pin tip radius [in]

params.h=0.026; % Height from pin axis to receptacle rotation point [in]
params.R=0.025; % Round of receptacle contact [in]
params.b=-0.007; % Receptacle arm end to R center (perpendicular) [in]
params.L=0.300; % Receptacle arm length [in]
params.K=0.004*453.592; % Angular stiffness [lbf*in/deg] to [grf*in/deg]
params.mu=0.20; % Friction coefficient [-]
params.theta0=0; % Initial imperfection in receptacle arm [deg]

d0=[.429;.222]; % Engaging separation and disengaging separation
dir=[1,-1]; % Same as {'engage','disengage'}

%% Solve for forces with respect to stroke
xl=[0,.21]; % Motion limits
x=[linspace(xl(1),xl(2),500),linspace(xl(2),xl(1),500)]; % Displacement [in]
vnorm=10*[ones(1,500),-ones(1,500)]; % Normalized velocity

% Get engaging (ii=1) and disengaging (ii=2) contacts via loop
for ii=1:2
    [Fx(ii,:),Fy(ii,:),Fn(ii,:),Ft(ii,:),theta(ii,:),Lmn(ii,:),...
        Lmt(ii,:),dcr(ii,:),thetacr(ii,:),xcr(ii,:),dc(ii),xc(ii)]=...
                            rec_pin_contact(x,params,vnorm,dir(ii),d0(ii));
end

%% Post-process

% Forces
fh(1)=figure;
ph1=plot(x,sum(Fx,1),'k-',x,sum(Fy,1),'b--',...
    reshape(xcr,1,[]),0*reshape(xcr,1,[]),'r.',xc,0*xc,'ro')
ylabel('Force [grf]');
xlabel('Displacement, x [in]')
```

```
xlim(xl);
legend(ph1,'F_x','F_y','x_{cr}','x_c','location','north');
legend boxoff
box off

fh(2)=figure;
ph2=plot(x,sum(Fn,1),'k-',x,sum(Ft,1),'b--',...
    reshape(xcr,1,[]),0*reshape(xcr,1,[]),'r.',xc,0*xc,'ro')
ylabel('Force [grf]');
xlabel('Displacement, x [in]')
xlim(xl);
legend(ph2,'F_n','F_t','x_{cr}','x_c','location','north');
legend boxoff
box off

% Other outputs (receptacle arm rotation, moment arms)
fh(3)=figure;
ph3=plot(x,sum(theta,1)*180/pi,...
    reshape(xcr,1,[]),0*reshape(xcr,1,[]),'r.',xc,0*xc,'ro')
ylabel('Receptacle Rotation, \theta [deg]')
xlabel('Displacement, x [in]')
xlim(xl);
legend(ph3,'\theta','x_{cr}','x_c','location','north');
legend boxoff
box off

fh(4)=figure;
ph4=plot(x,Lmn,'k-',x,Lmt,'b--',...
    reshape(xcr,1,[]),0*reshape(xcr,1,[]),'r.',xc,0*xc,'ro')
legend(ph4([1,3]),'L_{mn}','L_{mt}','x_{cr}','x_c','location','west');
legend boxoff
ylabel('Moment Arm [in]')
xlabel('Displacement, x [in]')
xlim(xl);
box off
```

Input Deck: Flexure and Round-Headed Pin

```
%% Flexure and Round-Headed Pin
close all
clear all

%% Define pin and receptacle geometry

params.Rr=0.015; % Pin round (ramp to barrel) [in]
params.Rp=0.015; % Pin barrel radius [in]
params.phi=45; % Pin ramp angle (pin axis to ramp) [deg]
params.Rt=0.015; % Pin tip radius [in]

params.h=0.081447; % Height from pin axis to receptacle rotation point [in]
params.R=0.035; % Round of receptacle contact [in]
params.b=-0.042447; % Receptecle arm end to R center (perpendicular) [in]
params.L=0.168; % Receptacle arm length [in]
params.K=0.00067*453.592; % Angular stiffness [lbf*in/deg] to [grf*in/deg]
params.mu=0.20; % Friction coefficient [-]
params.theta0=180; % Initial imperfection in receptacle arm [deg]
params.d0=-.048; % Initial separation from receptacle pivot to pin tip
params.dir='engage'; % Equivalent to 1, means engages with +x motion

%% Solve for forces with respect to stroke
xl=[0,0.2];
x=[linspace(xl(1),xl(2),500),linspace(xl(2),xl(1),500)]; % Displacement [in]
vnorm=10*[ones(1,500),-ones(1,500)]; % Normalized velocity

[Fx,Fy,Fn,Ft,theta,Lmn,Lmt,dcr,thetacr,xcr,dc,xc]=...
                                    rec_pin_contact(x,params,vnorm);

%% Post-process

% Forces
fh(1)=figure;
ph1=plot(x,Fx,'k-',x,Fy,'b--',xcr,0*xcr,'r.',xc,0*xc,'ro')
ylabel('Force [grf]');
xlabel('Displacement, x [in]')
xlim(xl);
legend(ph1,'F_x','F_y','x_{cr}','x_c','location','northwest');
legend boxoff
box off

fh(2)=figure;
ph2=plot(x,Fn,'k-',x,Ft,'b--',xcr,0*xcr,'r.',xc,0*xc,'ro')
ylabel('Force [grf]');
xlabel('Displacement, x [in]')
xlim(xl);
legend(ph2,'F_n','F_t','x_{cr}','x_c','location','northwest');
legend boxoff
box off

% Other outputs (receptacle arm rotation, moment arms)
fh(3)=figure;
ph3=plot(x,theta*180/pi,xcr,0*xcr,'r.',xc,0*xc,'ro')
```

```
ylabel('Receptacle Rotation, \theta [deg]')
xlabel('Displacement, x [in]')
xlim(xl);
legend(ph3,'\theta','x_{cr}','x_c','location','northwest');
legend boxoff
box off

fh(4)=figure;
ph4=plot(x,Lmn,'k-',x,Lmt,'b--',xcr,0*xcr,'r.',xc,0*xc,'ro')
legend(ph4,'L_{mn}','L_{mt}','x_{cr}','x_c','location','west');
legend boxoff
ylabel('Moment Arm [in]')
xlabel('Displacement, x [in]')
xlim(xl);
box off
```

DISTRIBUTION

1	MS0330	G.L. Artery	00427 (electronic copy)
1	MS0333	G.L. Benavides	02616 (electronic copy)
1	MS0333	S.A. Fillmore	02616 (electronic copy)
1	MS0333	D.E. Petersen	02616 (electronic copy)
1	MS0333	G.N. Rackley	02616 (electronic copy)
1	MS0333	R. Wild	02616 (electronic copy)
1	MS1064	R.S. Colbert	02615 (electronic copy)
1	MS1064	A.C. Hurst	02615 (electronic copy)
1	MS1064	P.T. Martin	02615 (electronic copy)
1	MS1064	J.T. McLaughlin	02615 (electronic copy)
1	MS1064	R.R. Parker	02615 (electronic copy)
1	MS0350	M.P. Sena	02615 (electronic copy)
1	MS0350	C. Siefert	02615 (electronic copy)
1	MS1064	L.M. Zsiga	02615 (electronic copy)
1	MS0350	M.P. Stevens	02614 (electronic copy)
1	MS0349	J.T. Bond	02613 (electronic copy)
1	MS0350	G.R. Ely	02613 (electronic copy)
1	MS0350	D. Groysman	02613 (electronic copy)
1	MS0350	S.C. Webb	02613 (electronic copy)
1	MS0343	C.W. Vanecek	02610 (electronic copy)
1	MS0346	D.E. Peebles	01526 (electronic copy)
1	MS1070	M.R. Brake	01526 (electronic copy)
1	MS1070	J.E. Massad	01526 (electronic copy)
1	MS1070	L. Zheng	01526 (electronic copy)
1	MS0899	Technical Library	9536 (electronic copy)

Page left intentionally blank


Sandia National Laboratories